What Do Electromagnetic Plasmas Tell Us about the Quark-Gluon Plasma?

Stanisław Mrówczyński[1] and Markus H. Thoma[2]

[1]Institute of Physics, Świętokrzyska Academy, PL-25-406 Kielce, Poland; and Sołtan Institute for Nuclear Studies, PL-00-681 Warsaw, Poland; email: mrow@fuw.edu.pl

[2]Max-Planck-Institute for Extraterrestrial Physics, D-85741 Garching, Germany; email: mthoma@mpe.mpg.de

Annu. Rev. Nucl. Part. Sci. 2007. 57:61–94

The *Annual Review of Nuclear and Particle Science* is online at http://nucl.annualreviews.org

This article's doi:
10.1146/annurev.nucl.57.090506.123124

0163-8998/07/1123-0061$20.00

Key Words

relativistic heavy-ion collisions

Abstract

Because the quark-gluon plasma (QGP) reveals some obvious similarities to the well-known electromagnetic plasma (EMP), an accumulated knowledge on EMPs can be used in QGP studies. After discussing similarities and differences of the two systems, we present the theoretical tools used to describe the plasmas. The tools include kinetic theory, hydrodynamic approach, and diagrammatic perturbative methods. We consider collective phenomena in the plasma, with a particular emphasis on instabilities that crucially influence the temporal evolution of the system. Finally, properties of strongly coupled plasma are discussed.

Contents

1. INTRODUCTION

Plasma—the ionized gas of electrons and ions—has been actively studied since its discovery in a discharge tube at the end of nineteenth century. The term plasma was introduced by Irving Langmuir in 1929. Prospects to get a practically unlimited source of energy due to nuclear fusion reactions in a hot ionized gas of hydrogen isotopes have stimulated a large-scale program to study plasmas in terrestrial experiments for more than half a century. Plasmas are also actively studied by astrophysicists, as it appears to be the most common phase of matter. Approximately 99% of the entire visible Universe is in the plasma phase. Not only are stars formed of ionized gas, but the interstellar and intergalactic mediums are also plasmas, although very sparse ones. Principles of plasma physics can be found in, for example, well-known textbooks (1, 2).

The quark-gluon plasma (QGP) is the system of quarks and gluons that are not confined in the hadron's interiors but can move freely in a whole volume occupied by the system. A broad presentation of the whole field of QGP physics is contained in three volumes of review articles (3–5); the lectures (6) can serve as an elementary introduction. Active studies of the QGP started in the mid-1980s when relativistic heavy-ion collisions offered an opportunity to create a drop of the QGP in a laboratory. The experimental programs at CERN and BNL provided evidence of the QGP production at the early stage of nucleus-nucleus collisions, when the system is extremely hot and dense, but properties of the QGP remain enigmatic. So, one can ask, what do electromagnetic plasmas (EMPs) tells us about the QGP?

The QGP reveals some obvious similarities to the well-known EMP, as quantum chromodynamics (QCD) describing the interactions of the quarks and gluons resembles quantum electrodynamics (QED), which governs interactions of charged objects. Thus, some lessons from EMPs should be useful in the exploration of the QGP. The aim of this review is to discuss what QGP physicists can actually learn from their EMP colleagues, and how the huge accumulated knowledge on EMPs

can be used in QGP studies. However, we must be aware not only of similarities but also of important differences between EMPs and the QGP. Some differences are of rather trivial origin, but some are deeply rooted in dynamical foundations of the two systems.

Let us enumerate these trivial dissimilarities. The QGP is usually relativistic or even ultrarelativistic, whereas the EMP is mostly nonrelativistic in laboratory experiments. The differences between the nonrelativistic and relativistic plasmas go far beyond the kinematics of motion of plasma particles. For example, let us consider the plasma's composition. In the nonrelativistic system, there are particles but no antiparticles, and the particle's number is conserved. In the relativistic system, we have both particles and antiparticles (as electrons and positrons in EMPs), and the lepton number—not the particle's number—is conserved. Particle number density is not a proper way to characterize the system. For this reason, QGP physicists use the baryon and strangeness densities.

Another trivial but very important distinctive feature of the EMP is the huge mass difference between electrons and ions, which is responsible for a specific dynamic role of heavy ions. The ions are usually treated as a passive background, which merely compensates the charge of electrons, but electro-ion collisions drive the system toward equilibrium and maintain the equilibrium. However, the energy transfer between electrons and ions is very inefficient, and their mutual equilibration is very slow. Therefore, we have electron and ion fluids of different temperatures for a relatively long time. There is nothing similar in the QGP. There are heavy quarks—charm, bottom, and top—that are, however, much less populated than the light quarks and gluons, and their lifetime is short. Therefore, the heavy quarks hardly influence the QGP dynamics.

The EMP, which is the closest analog of the QGP, is the relativistic system of electrons, positrons, and photons. Such a plasma is actually studied in the context of some astrophysical applications, for example, supernovae explosions. The differences between the QGP and the EMP are of dynamical origin: The first one is governed by QCD and the second one by QED. The latter theory is Abelian, whereas the former one is non-Abelian with a prominent role for gluons that carry color charges and, thus, not only mediate the interaction among colored quarks and antiquarks but interact among themselves. Gluons, in contrast to photons, also contribute to the density of color charges and to the color current.

The most important common feature of the EMP and the QGP is the collective character of the dynamics. The range of electrostatic interaction is, in spite of the screening, usually much larger than the interparticle spacing. There are many particles in the Debye sphere—the sphere of the radius equal to the effective interaction range—and motion of these particles is highly correlated. There is a similar situation in the deconfined perturbative phase of QCD (7). The Debye mass is of order gT, where g is the QCD constant and T is the temperature. Because the particle density in QGP is of order T^3, the number of partons in the Debye sphere, which is roughly $1/g^3$, is large in the weakly coupled ($1/g \gg 1$) QGP.

In various laboratory experiments, the EMP is embedded in an external electromagnetic field. For example, the magnetic field is used to trap the plasma, and there

are numerous fascinating phenomena occurring in such a situation. In the case of QGPs produced in relativistic heavy-ion collisions, it is hard to imagine any external chromodynamic field applied to the plasma. Therefore, we consider here only the systems in which fields are generated self-consistently in the plasma.

Our review is organized as follows: Theoretical tools, which are used to describe the plasmas, are presented in Section 2. The tools include the kinetic theory, the hydrodynamic approach, and diagrammatic methods of field theory. In Section 3 we discuss collective phenomena that are the most characteristic feature of plasmas. After explaining the phenomenon of screening, quasi-particle modes in the equilibrium and nonequilibrium plasma are presented. We pay much attention to instabilities that crucially influence plasma dynamics. The problem of a particle's energy loss in a plasma is also discussed. Section 4 is devoted to the strongly coupled plasma, which reveals particularly interesting properties.

Throughout the review we use the natural units, with $c = \hbar = k_B = 1$ and the metric $(1, -1, -1, -1)$. However, this gets a bit complicated. Plasma physicists usually use the Gauss (CGS) units, where the fine structure constant equals $\alpha = e^2 \approx 1/137$, and the electromagnetic counterpart of the units usually applied in QCD is the so-called Heaviside-Lorentz system, where the 4π factor does not show up in the Maxwell equations but $\alpha = e^2/4\pi$. We stick to the traditionally used units in the two fields of physics, and thus the factor of 4π must be additionally taken into account when comparing EMP and QGP formulas.

2. THEORETICAL TOOLS

2.1. Transport Theory

Transport theory provides a natural framework for studying equilibrium and nonequilibrium plasmas. The central object of the theory is the distribution function, which describes a time-dependent distribution of particles in a phase-space spanned by the particle's momenta and positions. The distribution function of each plasma component evolves owing to the interparticle collisions and the interaction with an external and/or self-consistently generated mean field. The two dynamical effects give rise to the collision and mean-field terms of a transport equation satisfied by the distribution function.

2.1.1. Electromagnetic plasma. A formulation of the kinetic theory of relativistic plasma can be found in Reference 8. The distribution function is denoted as $f_n(\mathbf{p}, x)$, with the index n labeling plasma components: electrons, positrons, ions. Spin is usually treated as an internal degree of freedom. The function depends on the four-position $x \equiv (t, \mathbf{x})$ and the three-momentum $\mathbf{p}$. The four-momentum p obeys the mass-shell constraint $p^2 = m^2$, where m is the particle mass. Then $p \equiv (E_p, \mathbf{p})$, with $E_p \equiv \sqrt{m^2 + \mathbf{p}^2}$.

The distribution function satisfies the transport equation

$$\left(p_\mu \partial^\mu + q_n p^\mu F_{\mu\nu} \partial_p^\nu\right) f_n(\mathbf{p}, x) = C[f_n], \qquad 1.$$

where $C[f_n]$ denotes the collision term, q_n is the charge of the plasma species n, and $F^{\mu\nu}$ is the electromagnetic strength tensor that either represents an external field applied to the system and/or is generated self-consistently by the four currents present in the plasma:

$$\partial^\mu F_{\mu\nu} = 4\pi j_\nu,$$

where

$$j^\mu(x) = \sum_n q_n \int \frac{d^3p}{(2\pi)^3} \frac{p^\mu}{E_p} f_n(\mathbf{p}, x). \quad 2.$$

The transport equation can be solved in the linear-response approximation. The equation is linearized around the stationary and homogeneous state described by the distribution $\bar{f}_n(\mathbf{p})$. The state is also assumed to be neutral, and there are no currents. The distribution function is then decomposed as

$$f_n(\mathbf{p}, x) = \bar{f}_n(\mathbf{p}) + \delta f_n(\mathbf{p}, x),$$

where $\bar{f}_n(\mathbf{p}) \gg \delta f_n(\mathbf{p}, x)$.

The transport equation linearized in δf_n, and $F^{\mu\nu}$ can be exactly solved after the Fourier transformation, which is defined as

$$f(k) = \int d^4x e^{ikx} f(x), \quad f(x) = \int \frac{d^4k}{(2\pi)^4} e^{-ikx} f(k). \quad 3.$$

Then, one finds $\delta f_n(\mathbf{p}, k)$, which is the Fourier transform of $\delta f_n(\mathbf{p}, x)$, and the induced current, which can be written as

$$\delta j^\mu(k) = -\Pi^{\mu\nu}(k) A_\nu(k), \quad 4.$$

with the polarization tensor equal to

$$\Pi^{\mu\nu}(k) = 4\pi \sum_n q_n^2 \int \frac{d^3p}{(2\pi)^3} \bar{f}_n(\mathbf{p}) \frac{(p\cdot k)^2 g^{\mu\nu} + k^2 p^\mu p^\nu - (p\cdot k)(k^\mu p^\nu + k^\nu p^\mu)}{(p\cdot k)^2}. \quad 5.$$

The tensor is symmetric [$\Pi^{\mu\nu}(k) = \Pi^{\nu\mu}(k)$] and transverse [$k_\mu \Pi^{\mu\nu}(k) = 0$], which guarantees that the current given by Equation 4 is gauge independent.

For isotropic plasmas, the polarization tensor has only two independent components, which are usually chosen as

$$\Pi_L(k) = \Pi_{00}(k)$$
$$\Pi_T(k) = \frac{1}{2}\left(\delta_{ij} - \frac{k_i k_j}{\mathbf{k}^2}\right)\Pi_{ij}(k), \quad 6.$$

where the indices $i, j = 1, 2, 3$ label three-vector and tensor components. In the case of an ultrarelativistic ($T \gg m$) electron-positron equilibrium plasma, the momentum integral in Equation 5 can be performed analytically in the high-temperature limit

($T \gg \omega, |\mathbf{k}|$), and the result already derived by Silin (9) in 1960 reads

$$\Pi_L(k) = -3m_\gamma^2 \left[1 - \frac{\omega}{2|\mathbf{k}|} \ln \frac{\omega + |\mathbf{k}|}{\omega - |\mathbf{k}|}\right],$$
$$\Pi_T(k) = \frac{3}{2} m_\gamma^2 \frac{\omega^2}{\mathbf{k}^2} \left[1 - \left(1 - \frac{\mathbf{k}^2}{\omega^2}\right) \frac{\omega}{2|\mathbf{k}|} \ln \frac{\omega + |\mathbf{k}|}{\omega - |\mathbf{k}|}\right], \quad 7.$$

where $k \equiv (\omega, \mathbf{k})$ and $m_\gamma \equiv eT/3$ denotes the thermal photon mass generated by the interaction of the photons with the electrons and positrons.

The above polarization tensor was found in the collisionless limit of the transport equation. The effect of collisions can be easily taken into account if the so-called Bhatnagar-Gross-Krook (BGK) collision term is used in the transport equation (Equation 10). The result for an ultrarelativistic equilibrium plasma is given in Reference 11.

2.1.2. Quark-gluon plasma. The transport theory of the QGP (12, 13) appears to be much more complicated than its electromagnetic counterpart. The distribution function of quarks $Q(\mathbf{p}, x)$ is a hermitian $N_c \times N_c$ matrix in color space [for an SU(N_c) color gauge group]. The distribution function is gauge dependent, and it transforms under a local gauge transformation $U(x)$ as

$$Q(\mathbf{p}, x) \to U(x) Q(\mathbf{p}, x) U^\dagger(x). \quad 8.$$

Here and in most cases below, the color indices are suppressed. The distribution function of antiquarks, which we denote by $\tilde{Q}(\mathbf{p}, x)$, is also a hermitian $N_c \times N_c$ matrix, and it transforms according to Equation 8. The distribution function of gluons is a hermitian $(N_c^2 - 1) \times (N_c^2 - 1)$ matrix, which transforms as

$$G(\mathbf{p}, x) \to \mathcal{U}(x) G(\mathbf{p}, x) \mathcal{U}^\dagger(x), \quad 9.$$

where

$$\mathcal{U}_{ab}(x) = 2\mathrm{Tr}[\tau^a U(x) \tau^b U^\dagger(x)],$$

with $\tau^a, a = 1, \ldots, N_c^2 - 1$ being the SU(N_c) group generators in the fundamental representation with $\mathrm{Tr}(\tau^a \tau^b) = \frac{1}{2}\delta^{ab}$.

The color current is expressed in the fundamental representation as

$$j^\mu(x) = -\frac{g}{2} \int \frac{d^3p}{(2\pi)^3} p^\mu \left[Q(\mathbf{p}, x) - \tilde{Q}(\mathbf{p}, x)\right]$$
$$- \frac{1}{N_c} \mathrm{Tr}\left[Q(\mathbf{p}, x) - \tilde{Q}(\mathbf{p}, x)\right] + 2\tau^a \mathrm{Tr}\left[T^a G(\mathbf{p}, x)\right], \quad 10.$$

where g is the QCD coupling constant. A sum over helicities, two per particle, and over quark flavors N_f is understood in Equation 10, even though it is not explicitly written down. The SU(N_c) generators in the adjoint representation are expressed through the structure constants $T^a_{bc} = -if_{abc}$, and are normalized as $\mathrm{Tr}[T^a T^b] = N_c \delta^{ab}$. The current can be decomposed as $j^\mu(x) = j^\mu_a(x)\tau^a$, with $j^\mu_a(x) = 2\mathrm{Tr}(\tau_a j^\mu(x))$. The distribution functions, which are proportional to the unit

matrix in color space, are gauge independent, and they provide the color current (Equation 10) that vanishes identically.

Gauge-invariant quantities are given by the traces of the distribution functions. Thus, the baryon current and the energy-momentum tensor read

$$b^\mu(x) = \frac{1}{3}\int \frac{d^3p}{(2\pi)^3} p^\mu \mathrm{Tr}\left[Q(\mathbf{p},x) - \tilde{Q}(\mathbf{p},x)\right],$$
$$T^{\mu\nu}(x) = \int \frac{d^3p}{(2\pi)^3} p^\mu p^\nu \mathrm{Tr}\left[Q(\mathbf{p},x) + \tilde{Q}(\mathbf{p},x) + G(\mathbf{p},x)\right],$$

where we use the same symbol $\mathrm{Tr}[\cdots]$ for the trace both in the fundamental and adjoint representations.

The distribution functions of quarks, antiquarks, and gluons satisfy the transport equations

$$p^\mu D_\mu Q(\mathbf{p},x) + \frac{g}{2} p^\mu \left\{F_{\mu\nu}(x), \partial_p^\nu Q(\mathbf{p},x)\right\} = C[Q,\tilde{Q},G], \quad 11.$$

$$p^\mu D_\mu \tilde{Q}(\mathbf{p},x) - \frac{g}{2} p^\mu \left\{F_{\mu\nu}(x), \partial_p^\nu \tilde{Q}(\mathbf{p},x)\right\} = \tilde{C}[Q,\tilde{Q},G], \quad 12.$$

$$p^\mu D_\mu G(\mathbf{p},x) + \frac{g}{2} p^\mu \left\{\mathcal{F}_{\mu\nu}(x), \partial_p^\nu G(\mathbf{p},x)\right\} = C_g[Q,\tilde{Q},G], \quad 13.$$

where $\{\ldots,\ldots\}$ denotes the anticommutator and ∂_p^ν the four-momentum derivative.[1] The covariant derivatives D_μ and $\mathcal{D}_\mu$ act as

$$D_\mu = \partial_\mu - ig[A_\mu(x),\ldots], \quad \mathcal{D}_\mu = \partial_\mu - ig[\mathcal{A}_\mu(x),\ldots],$$

with A_μ and $\mathcal{A}_\mu$ being four-potentials in the fundamental and adjoint representations, respectively:

$$A^\mu(x) = A_a^\mu(x)\tau^a, \quad \mathcal{A}^\mu(x) = T^a A_a^\mu(x).$$

The strength tensor in the fundamental representation is $F_{\mu\nu} = \partial_\mu A_\nu - \partial_\nu A_\mu - ig[A_\mu, A_\nu]$, whereas $\mathcal{F}_{\mu\nu}$ denotes the field strength tensor in the adjoint representation. C, $\tilde{C}$ and C_g represent the collision terms.

The transport equations are supplemented by the Yang-Mills equation describing generation of the gauge field:

$$D_\mu F^{\mu\nu}(x) = j^\nu(x), \quad 14.$$

where the color current is given by Equation 10. As in the case of the electromagnetic plasma, the transport equations, which are linearized around a stationary, homogeneous, and colorless state, can be solved. Because of the color neutrality assumption, the analysis is rather similar to that of the Abelian plasma, and it ends up with the polarization tensor that is proportional to the unit matrix in the color space and has the form of Equation 5.

[1] As the distribution functions do not depend on p_0, the derivative over p_0 is identically zero.

As in the case with EMPs, the collisions can be easily taken into account using the approximate BGK collision terms (14, 15). Within a more realistic approach, color charges are treated in a similar way as spin degrees of freedom, and one uses the so-called Waldmann-Snider collision terms (16, 17), which are usually applied to study spin transport.

2.2. Hydrodynamic Approach

Within the hydrodynamic approach, the plasma is treated as a liquid and described in terms of macroscopic variables that obey the equations of motion resulting from the conservation laws. The fluid equations are applied to a large variety of plasma phenomena, but, depending of the timescale of interest, the actual physical content of the equations is rather different.

Real hydrodynamics deals with systems in local equilibrium, and thus it is applicable only at sufficiently long timescales. The continuity and the Euler or Navier-Stokes equations are supplemented by the equation of state to form a complete set of equations. The equations can be derived from kinetic theory, using the distribution function of local equilibrium, which by definition maximizes the entropy density and thus cancels the collision terms of the transport equations.

In the electron-ion plasma, there are several timescales of equilibration. The electron component of the plasma reaches the equilibrium in the shortest time. Then ions are equilibrated, but for a relatively long time the electron and ion temperatures remain different from each other, as the energy transfer between electrons to ions is rather inefficient. This happens owing to the huge mass difference between electrons and ions.

When the electrons have reached local equilibrium with their own temperature and hydrodynamic velocity, the collision terms of the kinetic equations representing electron-electron collisions vanish, while the collision terms due to electron-ion collisions can be neglected because they influence the electron distribution function only at a sufficiently long timescale. Then, one obtains hydrodynamic equations of an electron fluid. When the ion component is also equilibrated, we have two fluids with different temperatures and hydrodynamic velocities. At the timescales when the fluid equations are applicable, the plasma can be treated as locally neutral. Charge fluctuations are obviously possible, but they disappear rapidly because the electric field generated by the local charges induces the currents, which in turn neutralize the charges. Because the plasma is nearly an ideal conductor, the process of plasma neutralization is very fast. Owing to the charge neutrality of the plasma, the electric field is not present in the fluid equations and we end up with magnetohydrodynamics, where the pressure gradients and magnetic field drive the plasma dynamics.

As explained above, the regime of magnetohydrodynamics appears because there is a heavy positive component (ions) and a light negative component (electrons) of the plasma. There is no QCD analog of magnetohydrodynamics, as every quark or gluon can carry opposite color charges. Therefore, when local equilibrium is reached, various color components of the plasma have the same temperatures and hydrodynamic velocities (17). Because the quark-gluon system becomes color neutral even before

the local equilibration is reached (14, 16), we deal with hydrodynamics of a neutral fluid where the chromodynamic fields are absent. Such a relativistic hydrodynamics of colorless QGP has been actively studied over the past two decades (18, 19).

The hydrodynamic equations, which actually express macroscopic conservation laws, hold not only for systems in local equilibrium but for systems out of equilibrium as well. The equations can then be applied at timescales significantly shorter than that of local equilibration. At such a short timescale, the collision terms of the transport equations can be neglected entirely. However, extra assumptions are then needed to close the set of equations, as the (equilibrium) equation of state cannot be used. Plasma physicists developed several methods to close the set of equations, and thus fluid equations are used to study bulk features of short timescale phenomena in the plasmas. To get more detailed information, kinetic theory is needed. Because the fluid equations are noticeably simpler than the kinetic ones, the hydrodynamic approach is used frequently in numerical simulations of plasma evolution, studies of nonlinear dynamics, and so on.

Below, we derive the fluid equations for the EMP and the QGP from the respective kinetic theory. Because the fluid approach under consideration is supposed to hold at sufficiently short timescales, we use the collisionless transport equations.

2.2.1. Electromagnetic plasma. We assume here that there are several streams in the relativistic plasma system and that the distribution functions of each plasma component (electrons, positrons, ions) belonging to each stream satisfy the collisionless transport equation. The equations are coupled only through the electromagnetic mean field, which is generated by the current coming from all streams. The field in turn interacts with every stream.

Integrating the collisionless transport equation (Equation 1) over momentum, one finds the continuity equation

$$\partial_\mu n^\mu_\alpha = 0, \tag{15.}$$

where the four-flow is

$$n^\mu_\alpha(x) \equiv \int \frac{d^3p}{(2\pi)^3} p^\mu f_\alpha(\mathbf{p}, x). \tag{16.}$$

The index α simultaneously labels the streams and plasma components.

Multiplying the transport equation (Equation 1) by the four-momentum p and integrating over momentum, we get

$$\partial_\mu T^{\mu\nu}_\alpha + q_\alpha n^\mu_\alpha F^\nu_\mu = 0, \tag{17.}$$

where the energy-momentum tensor is

$$T^{\mu\nu}_\alpha(x) \equiv \int \frac{d^3p}{(2\pi)^3} p^\mu p^\nu f_\alpha(\mathbf{p}, x). \tag{18.}$$

The structure of n^μ_α and $T^{\mu\nu}_\alpha$ is assumed to be that of an ideal fluid in local thermodynamic equilibrium. Thus, one has

$$n^\mu_\alpha(x) = n_\alpha(x) u^\mu_\alpha(x), \tag{19.}$$

$$T^{\mu\nu}_\alpha(x) = [\varepsilon_\alpha(x) + p_\alpha(x)]\, u^\mu(x) u^\nu(x) - p_\alpha(x) g^{\mu\nu}. \tag{20.}$$

To obtain the relativistic version of the Euler equation, Equation 17 needs to be manipulated following Reference 20. Substituting the energy-momentum tensor of the form of Equation 20 into Equation 17 and projecting the result on the direction of u_α^μ, one finds

$$u_{\alpha\nu}\partial_\mu T_\alpha^{\mu\nu} = u_\alpha^\mu \partial_\mu \varepsilon_\alpha + (\varepsilon_\alpha + p_\alpha)\partial_\mu u_\alpha^\mu = 0. \qquad 21.$$

Computing $\partial_\mu T_\alpha^{\mu\nu} - u_\alpha^\nu u_{\alpha\rho}\partial_\mu T_\alpha^{\mu\rho}$, one gets the Lorentz covariant form of the Euler equation

$$M_\alpha^\nu \equiv (\varepsilon_\alpha + p_\alpha)u_{\alpha\mu}\partial^\mu u_\alpha^\nu + \left(u_\alpha^\mu u_\alpha^\nu \partial_\mu - \partial^\nu\right) p - q_\alpha n_\alpha u_{\alpha\mu} F^{\mu\nu} = 0. \qquad 22.$$

In a more familiar form, the equation is given by $\mathbf{M}_\alpha - \mathbf{v}_\alpha M_\alpha^0 = 0$. Namely,

$$(\varepsilon_\alpha + p_\alpha)\gamma_\alpha^2 \left(\frac{\partial}{\partial t} + \mathbf{v}_\alpha \cdot \nabla\right)\mathbf{v}_\alpha + \left(\nabla + \mathbf{v}_\alpha \frac{\partial}{\partial t}\right) p_\alpha - q_\alpha n_\alpha \gamma_\alpha \left[\mathbf{E} - \mathbf{v}_\alpha(\mathbf{v}_\alpha \cdot \mathbf{E}) + \mathbf{v}_\alpha \times \mathbf{B}\right] = 0, \qquad 23.$$

where the four-velocity u_α^μ was expressed as $u_\alpha^\mu = (\gamma_\alpha, \gamma_\alpha \mathbf{v}_\alpha)$, with $\gamma_\alpha \equiv (1 - \mathbf{v}_\alpha^2)^{-1/2}$.

In the nonrelativistic limit (which is easily obtained when the velocity of light c is restored in the equation), Equation 23 assumes the well-known form

$$\left(\frac{\partial}{\partial t} + \mathbf{v}_\alpha \cdot \nabla\right)\mathbf{v}_\alpha + \frac{1}{m_\alpha n_\alpha}\nabla p_\alpha - \frac{q_\alpha}{m_\alpha}(\mathbf{E} + \mathbf{v}_\alpha \times \mathbf{B}) = 0. \qquad 24.$$

The fluid Equations 15 and 17 with n_α^μ and $T_\alpha^{\mu\nu}$ given by Equations 19 and 20, respectively, do not constitute a closed set of equations. There are five equations and six unknown functions: n_α, p_α, ε_α, and three components of u_α^μ (because of the constraint $u_\alpha^\mu u_{\mu\,\alpha} = 1$, one component of u_α^μ can be eliminated). There are several methods to close the set of equations. In particular, assuming that the system's dynamics is dominated by the mean-field interaction, one can neglect the pressure gradients. One can also add an equation that relates p_α to ε_α. The relation is usually known as the equation of state, but one should be aware that the plasma system is not in equilibrium, and in general the thermodynamic relations do not hold.

In the ultrarelativistic limit when the characteristic particle's energy (the temperature of the equilibrium system) is much larger than the particle's mass, and thus $p^2 \cong 0$, the energy-momentum tensor is traceless ($T_{\mu\alpha}^\mu = 0$), as follows from Equation 18 for $p^2 = 0$. Then, Equation 20 combined with the constraint $u_\alpha^\mu(x)u_{\alpha\mu}(x) = 1$ provides the desired relation

$$\varepsilon_\alpha(x) = 3\,p_\alpha(x), \qquad 25.$$

which coincides with the equation of state of an ideal gas of massless particles.

Because the distribution functions of every plasma component belonging to every stream are assumed to obey the collisionless transport equation, we have a separated set of fluid equations for every plasma component of every stream. The equations are coupled only through the electromagnetic mean field. More precisely, the electrons, positrons, and ions of every stream contribute to the current generating the field, which in turn interacts with the streams.

The fluid equations can be solved in the linear-response approximation. The equations are linearized around the stationary and homogeneous state described by $\bar{n}_\alpha$ and

$\bar{u}^{\mu}_{\alpha}$. This state is neutral and there are no currents, i.e.,

$$\sum_{\alpha} \bar{n}_{\alpha} \bar{u}^{\mu}_{\alpha} = 0. \tag{26.}$$

The charge density is decomposed as

$$n_{\alpha}(x) = \bar{n}_{\alpha} + \delta n_{\alpha}(x), \tag{27.}$$

where $\bar{n}_{\alpha} \gg \delta n_{\alpha}$. The fully analogous decomposition of the hydrodynamic velocity u^{μ}_{α}, pressure p_{α}, and energy density ε_{α} is also adopted.

The set of the continuity and Euler equations linearized in δn_{α}, δu^{μ}_{α}, δp_{α}, $\delta \varepsilon_{\alpha}$, and $F^{\mu\nu}$ can be exactly solved after they are Fourier transformed. Thus, one finds $\delta n_{\alpha}(k)$ and $\delta u^{\mu}_{\alpha}(k)$ when the set of fluid equations is closed by neglecting the pressure gradients. If the equation of state is used, one also finds $\delta \varepsilon_{\alpha}(k)$.

Keeping in mind that the induced current equals

$$\delta j^{\mu} = \sum_{\alpha} \left(q_{\alpha} \bar{n}_{\alpha} \delta u^{\mu}_{\alpha} + q_{\alpha} \delta n_{\alpha} \bar{u}^{\mu}_{\alpha} \right),$$

one finds from Equation 4

$$\Pi^{\mu\nu}(k) = \sum_{\alpha} \frac{4\pi q_{\alpha}^2 \bar{n}_{\alpha}^2}{\bar{\varepsilon}_{\alpha} + \bar{p}_{\alpha}} \frac{1}{(\bar{u}_{\alpha} \cdot k)^2} \left[k^2 \bar{u}^{\mu}_{\alpha} \bar{u}^{\nu}_{\alpha} + (\bar{u}_{\alpha} \cdot k)^2 g^{\mu\nu} - (\bar{u}_{\alpha} \cdot k) \left(k^{\mu} \bar{u}^{\nu}_{\alpha} + k^{\mu} \bar{u}^{\mu}_{\alpha} \right) \right.$$
$$\left. + \frac{(\bar{u}_{\alpha} \cdot k) k^2 \left(k^{\mu} \bar{u}^{\nu}_{\alpha} + k^{\nu} \bar{u}^{\mu}_{\alpha} \right) - (\bar{u}_{\alpha} \cdot k)^2 k^{\mu} k^{\nu} - k^4 \bar{u}^{\mu}_{\alpha} \bar{u}^{\nu}_{\alpha}}{k^2 + 2(\bar{u}_{\alpha} \cdot k)^2} \right] \tag{28.}$$

The first term gives the polarization tensor when the pressure gradients are neglected, and the second term gives the effect of the pressure gradients due to the equation of state given by Equation 25. The first term is symmetric [$\Pi^{\mu\nu}(k) = \Pi^{\nu\mu}(k)$] and transverse [$k_{\mu} \Pi^{\mu\nu}(k) = 0$]. The second term is symmetric and transverse as well. Thus, the whole polarization tensor (Equation 28) is symmetric and transverse. The first term of Equation 28 can be obtained from the kinetic theory result (Equation 5) with the distribution function $\bar{f}_n(\mathbf{p})$ proportional to $\delta^{(3)}(\mathbf{p} - (\bar{\varepsilon}_{\alpha} + \bar{p}_{\alpha})\mathbf{u}_{\alpha}/\bar{n}_{\alpha})$. Thus, the first term neglects the thermal motion of plasma particles, whereas the second term takes this effect into account.

2.2.2. Quark-gluon plasma. The fluid approach presented here follows the formulation given in Reference 21. As in the EMP case, we assume that there are several streams in the plasma system and that the distribution functions of quarks, antiquarks, and gluons of each stream satisfy the collisionless transport equation. The streams are labeled with the index α.

Further analysis is limited to quarks, but inclusion of antiquarks and gluons is straightforward. The distribution function of quarks belonging to the stream α is denoted as $Q_{\alpha}(\mathbf{p}, x)$. Integrating over momentum—the collisionless transport (Equation 11) satisfied by Q_{α}—one finds the covariant continuity equation

$$D_{\mu} n^{\mu}_{\alpha} = 0, \tag{29.}$$

where n^μ_α is an $N_c \times N_c$ matrix defined as

$$n^\mu_\alpha(x) \equiv \int \frac{d^3p}{(2\pi)^3} p^\mu Q_\alpha(\mathbf{p}, x). \tag{30.}$$

The four-flow n^μ_α transforms under gauge transformations as the quark distribution function, that is, according to Equation 8.

Multiplying the transport (Equation 11) by the four-momentum and integrating the product over momentum, we obtain

$$D_\mu T^{\mu\nu}_\alpha - \frac{g}{2}\left\{F^\nu_\mu, n^\mu_\alpha\right\} = 0, \tag{31.}$$

where the energy-momentum tensor is

$$T^{\mu\nu}_\alpha(x) \equiv \int \frac{d^3p}{(2\pi)^3} p^\mu p^\nu Q_\alpha(\mathbf{p}, x). \tag{32.}$$

We assume further that the structure of n^μ_α and $T^{\mu\nu}_\alpha$ is

$$n^\mu_\alpha(x) = n_\alpha(x) u^\mu_\alpha(x), \tag{33.}$$

$$T^{\mu\nu}_\alpha(x) = \frac{1}{2}\left(\varepsilon_\alpha(x) + p_\alpha(x)\right)\left\{u^\mu_\alpha(x), u^\nu_\alpha(x)\right\} - p_\alpha(x) g^{\mu\nu}, \tag{34.}$$

where the hydrodynamic velocity u^μ_α is, as n_α, ε_α, and p_α, an $N_c \times N_c$ matrix. The anticommutator of u^μ_α and u^ν_α is present in Equation 34 to guarantee the symmetry of $T^{\mu\nu}_\alpha$ with respect to $\mu \leftrightarrow \nu$, which is evident in Equation 32.

In the case of an Abelian plasma, the relativistic version of the Euler equation is obtained from Equation 31 by removing from it the component parallel to u^μ_α. An analogous procedure is not possible for the non-Abelian plasma because in general the matrices n_α, u^μ_α, and u^ν_α do not commute with each other. Thus, one has to work directly with Equations 29 and 31 with n^μ_α and $T^{\mu\nu}_\alpha$ defined by Equations 33 and 34, respectively. The equations have to be supplemented by the Yang-Mills equation (Equation 14) with the color current of the form

$$j^\mu(x) = -\frac{g}{2}\sum_\alpha \left(n_\alpha u^\mu_\alpha - \frac{1}{N_c}\mathrm{Tr}\left[n_\alpha u^\mu_\alpha\right]\right), \tag{35.}$$

where only the quark contribution is taken into account.

The fluid Equations 29 and 31, as their electromagnetic counterpart, do not form a closed set of equations, but can be closed analogously. The only difference is that the equation of state (Equation 25) relates the matrix value functions ε_α and p_α to each other.

As in the case of the electromagnetic plasma, the fluid Equations 15 and 17, which are linearized around a stationary, homogeneous, and colorless state described by $\bar{n}_\alpha$, $\bar{\varepsilon}_\alpha$, $\bar{p}_\alpha$, and $\bar{u}^\mu_\alpha$ can be solved (21). Because of the color-neutrality assumption—$\bar{n}_\alpha$, $\bar{\varepsilon}_\alpha$, $\bar{p}_\alpha$, and $\bar{u}^\mu_\alpha$ are all proportional to the unit matrix in the color space—the analysis is rather similar to that of the Abelian plasma, and one ends up with the polarization tensor from Equation 28, which is proportional to the unit matrix in the color space.

2.3. Diagrammatic Methods

Various characteristics of the weakly coupled plasma can be calculated using the perturbative expansion, that is, diagrammatic methods of field theory. It requires a generalization of the Feynman rules applicable to processes, which occur in vacuum, to many-body plasma systems. When the plasma is in thermodynamic equilibrium, one can either follow the so-called imaginary-time formalism (see, e.g., References 22 and 23) or the real-time (Schwinger-Keldysh) formalism (24, 25). The latter can also be extended to nonequilibrium situations (26, 27).

The perturbative expansion expressed in terms of Feynman diagrams allows a systematic computation of various quantities. However, to obtain a gauge-invariant finite result, one often has to re-sum a class of diagrams, as required by the hard loop approach (28–30) (the real-time formulation is discussed in Reference 31). The approach, which was first developed for equilibrium systems (28–30) (for a review, see Reference 32) and then extended to the nonequilibrium case (33–35), distinguishes soft from hard momenta. In the case of ultrarelativistic QED plasmas in equilibrium, the soft momenta are of order eT, whereas the hard momenta are of order T, with T being the plasma temperature. One obviously assumes that $1/e \gg 1$. The hard loop approach deals with soft collective excitations generated by hard plasma particles that dominate the distribution functions.

As an example, we consider the polarization tensor given by Equation 5, which was obtained within the kinetic theory in Section 2.1. We restrict ourselves to ultrarelativistic QED plasmas. In the lowest order of the perturbative expansion, the polarization tensor or photon self-energy is given by the diagram shown in **Figure 1**. The tensor can be decomposed into vacuum and medium contributions. The first one requires a usual renormalization because of a UV divergence, whereas the medium part appears to be UV finite. One reproduces Equation 5 by applying to the diagrammatic result the hard loop approximation, which requires that the energy and momentum (ω, $\mathbf{k}$) of the external photon line are much smaller than the momentum ($\mathbf{p}$) of the electron loop. Then, it appears that the vacuum part can be neglected, as it is much smaller than the medium part. In the case of an ultrarelativistic equilibrium EMP, Equation 7 was derived diagrammatically in References 36 and 37. In the QGP, the lowest-order polarization tensor (gluon self-energy) includes one-loop diagrams with internal gluon and ghost lines. The final result for the gluon-polarization tensor in the high-temperature approximation essentially coincides with the QED expression. The color degrees of freedom enter through the trivial color factor δ_{ab}. In the case of equilibrium QGP, one additionally replaces in Equation 7 the thermal photon

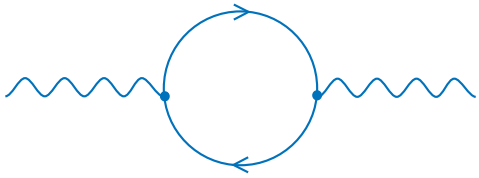

Figure 1

The lowest-order contribution to the QED polarization tensor.

mass by a thermal gluon mass given by

$$m_g^2 = \frac{g^2 T^2}{3}\left(1 + \frac{N_f}{6}\right), \qquad 36.$$

where N_f indicates the number of light-quark flavors.

The hard loop approach can be formulated nicely in terms of an effective action. Such an action for an equilibrium system was derived diagrammatically in Reference 29 and in the explicitly gauge-invariant form in Reference 30. The equilibrium hard loop action was also found within the semiclassical kinetic theory (38, 39). The action was generalized (33, 35) for nonequilibrium systems, which are, on average, locally color neutral, stationary, and homogeneous.

The starting point was the effective action, which describes an interaction of classical fields with currents induced by these fields in the plasma. The Lagrangian density is quadratic in the gluon and quark fields, and it equals

$$\mathcal{L}_2(x) = -\int d^4y \left[\frac{1}{2} A^a_\mu(x) \Pi^{\mu\nu}_{ab}(x-y) A^b_\nu(y) + \bar{\Psi}(x)\Sigma(x-y)\Psi(y)\right], \qquad 37.$$

where $\Pi^{\mu\nu}_{ab}$ and Σ are the gluon-polarization tensor and the quark self-energy, respectively, while A^a and Ψ denote the gluon and quark fields. Following Braaten & Pisarski (30), the Lagrangian from Equation 37 was modified to comply with the requirement of gauge invariance. The final result, which is nonlocal but manifestly gauge invariant, is

$$\mathcal{L}_{\mathrm{HL}}(x) = \frac{g^2}{2}\int \frac{d^3p}{(2\pi)^3}\left[f(\mathbf{p}) F^a_{\mu\nu}(x)\left(\frac{p^\nu p^\rho}{(p\cdot D)^2}\right)_{ab} F^{b\mu}_{\rho}(x) + i\frac{N_c^2-1}{4N_c}\tilde{f}(\mathbf{p})\bar{\Psi}(x)\frac{p\cdot\gamma}{p\cdot D}\Psi(x)\right], \qquad 38.$$

where $F^{\mu\nu}_a$ is the strength tensor and D denotes the covariant derivative; $f(\mathbf{p})$ and $\tilde{f}(\mathbf{p})$ are the effective parton distribution functions defined as $f(\mathbf{p}) \equiv n(\mathbf{p}) + \bar{n}(\mathbf{p}) + 2N_c n_g(\mathbf{p})$ and $\tilde{f}(\mathbf{p}) \equiv n(\mathbf{p}) + \bar{n}(\mathbf{p}) + 2n_g(\mathbf{p})$, respectively; $n(\mathbf{p})$, $\bar{n}(\mathbf{p})$, and $n_g(\mathbf{p})$ are the distribution functions of quarks, antiquarks, and gluons, respectively, of a single-color component in a homogeneous and stationary plasma, which is locally and globally colorless; the spin and flavor are treated as parton internal degrees of freedom. The quarks and gluons are assumed to be massless. The effective action given by Equation 38 generates n-point functions, which obey the Ward-Takahashi identities. Equation 38 holds under the assumption that the field amplitude is much smaller than T/g, where T denotes the characteristic momentum of (hard) partons.

3. COLLECTIVE PHENOMENA

The most characteristic feature of the electromagnetic and QCD plasmas, which results from a long-range interaction governing both systems, is a collective behavior that leads to specific plasma phenomena such as screening, plasma oscillations, instabilities, and so on.

Because the electromagnetic and chromodynamic polarization tensors, which are obtained in the linear-response analysis, are essentially the same, the collective effects in EMPs and QGPs are very similar in the linear-response regime. As our discussion is limited to this regime, mostly the EMP is considered in this section.

3.1. Screening

We start with screening of electric charges in the plasma. To discuss the effect, let us consider an electric field generated by a point-like charge q moving with velocity $\mathbf{v}$ in the plasma. The problem is studied in numerous plasma handbooks, for example, in Reference 2. The induction vector obeys the Maxwell equation

$$\nabla \cdot \mathbf{D}(x) = 4\pi q \delta^{(3)}(\mathbf{r} - \mathbf{v}t) \, ,$$

with $x \equiv (t, \mathbf{r})$. After the Fourier transformation, which is defined by Equation 3, the induction vector reads

$$i\mathbf{k} \cdot \mathbf{D}(k) = 8\pi^2 q \, \delta(\omega - \mathbf{k} \cdot \mathbf{v}), \qquad 39.$$

where $k \equiv (\omega, \mathbf{k})$. The induction vector $\mathbf{D}(k)$ is related to the electric field $\mathbf{E}(k)$ through the dielectric tensor $\varepsilon^{ij}(k)$ as

$$D^i(k) = \varepsilon^{ij}(k) E^j(k). \qquad 40.$$

We note that the dielectric tensor $\varepsilon^{ij}(k)$, which carries information on the electromagnetic properties of a medium, can be expressed through the polarization tensor as

$$\varepsilon^{ij}(k) = \delta^{ij} + \frac{1}{\omega^2} \Pi^{ij}(k). \qquad 41.$$

In an isotropic plasma, there are only two independent components of the dielectric tensor ε_T and ε_L, which are related to ε^{ij} as

$$\varepsilon^{ij}(k) = \varepsilon_T(k)(\delta^{ij} - k^i k^j / \mathbf{k}^2) + \varepsilon_L(k) k^i k^j / \mathbf{k}^2. \qquad 42.$$

Using Equations 40 and 42, and expressing the electric field $\mathbf{E}$ through the scalar ϕ and vector $\mathbf{A}$ potentials [$\mathbf{E}(k) = -i\mathbf{k}\phi(k) + i\omega\mathbf{A}(k)$] in the Coulomb gauge [$\mathbf{k} \cdot \mathbf{A}(k) = 0$], one finds the electric potential in a medium (the wake potential):

$$\phi(x) = 4\pi q \int \frac{d^3k}{(2\pi)^3} \frac{e^{i\mathbf{k}\cdot(\mathbf{r}-\mathbf{v}t)}}{\varepsilon_L(\omega = \mathbf{v} \cdot \mathbf{k}, \mathbf{k})\mathbf{k}^2}. \qquad 43.$$

Let us first consider the simplest case of the potential generated by a static ($\mathbf{v} = 0$) charge. Using Equations 6 and 7, $\varepsilon_L(0, \mathbf{k})$ of an ultrarelatvistic electron-positron plasma is found as

$$\varepsilon_L(0, \mathbf{k}) = 1 + \frac{m_D^2}{\mathbf{k}^2} \, , \qquad 44.$$

where m_D is the so-called Debye mass given by $m_D^2 = e^2 T^2/3 = 3m_\gamma^2 = \Pi_L(0, \mathbf{k})$. Then, Equation 43 gives the well-known screened potential

$$\phi(\mathbf{r}) = \frac{q}{r} e^{-m_D r}, \qquad 45.$$

with $r \equiv |\mathbf{r}|$. Thus, the inverse Debye mass has the interpretation of the screening length of the potential. Because the average interparticle spacing in the ultrarelativistic plasma is of order T^{-1}, the number of particles in the Debye sphere (the sphere of the radius m_D^{-1}) is of order e^{-3}, which is, as already mentioned in the Introduction, much larger than unity in the weakly coupled plasma ($1/e^2 \gg 1$). This explains the collective behavior of the plasma, since motion of particles from the Debye sphere is highly correlated.

For $\mathbf{v} \neq 0$, the potential given by Equation 43 has a rich structure. It has been discussed in the context of QGPs in References 40–42, showing that it can exhibit attractive contributions even between like-sign charges in certain directions (40). For a supersonic particle, the potential can reveal a Mach cone structure associated with Cerenkov radiation when electromagnetic properties of the plasma are appropriately modeled (41, 42).

3.2. Collective Modes

Let us consider a plasma in a homogenous, stationary state with no local charges and no currents. As a fluctuation or perturbation of this state, there appear local charges or currents generating electric and magnetic fields, which in turn interact with charged plasma particles. Then, the plasma reveals a collective motion, which classically is termed plasma oscillations. Quantum mechanically we deal with quasiparticle collective excitations of the plasma.

The collective modes are solutions of the dispersion equation obtained from the equation of motion of the Fourier-transformed electromagnetic potential $A^\mu(k)$, which is

$$[k^2 g^{\mu\nu} - k^\mu k^\nu - \Pi^{\mu\nu}(k)]A_\nu(k) = 0, \qquad 46.$$

where the polarization tensor $\Pi^{\mu\nu}$ contains all dynamical information about the system. The general dispersion equation is then

$$\det[k^2 g^{\mu\nu} - k^\mu k^\nu - \Pi^{\mu\nu}(k)] = 0. \qquad 47.$$

Owing to the transversality of $\Pi^{\mu\nu}(k)$, not all components of $\Pi^{\mu\nu}(k)$ are independent of each other. Consequently, the dispersion equation (Equation 47), which involves a determinant of a 4×4 matrix, can be simplified to the determinant of a 3×3 matrix. For this purpose, one usually introduces the dielectric tensor $\varepsilon^{ij}(k)$, which is related to the polarization tensor by Equation 41. Then, the dispersion equation gets the form

$$\det[\mathbf{k}^2 \delta^{ij} - k^i k^j - \omega^2 \varepsilon^{ij}(k)] = 0. \qquad 48.$$

The relationship between Equation 47 and Equation 48 is most easily seen in the Coulomb gauge when $\phi = 0$ and $\mathbf{k} \cdot \mathbf{A}(k) = 0$. Then, $\mathbf{E} = i\omega\mathbf{A}$ and Equation 46 is immediately transformed into an equation of motion for $\mathbf{E}(k)$, which further provides the dispersion equation (Equation 48).

As expressed by Equation 42, there are only two independent components of the dielectric tensor [$\varepsilon_T(k)$ and $\varepsilon_L(k)$] in an isotropic plasma. Then, the dispersion

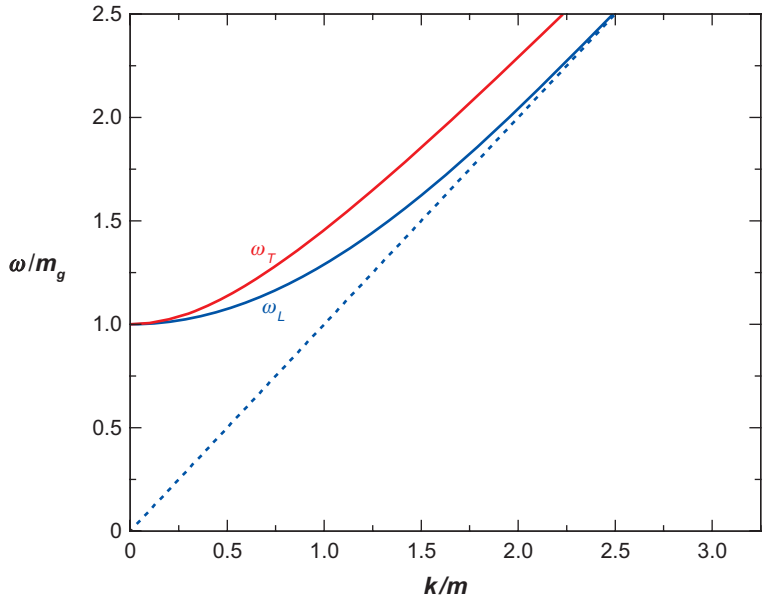

Figure 2

Dispersion relation of longitudinal and transverse plasma waves.

equation (Equation 48) splits into two equations:

$$\varepsilon_T(k) = \mathbf{k}^2/\omega^2, \quad \varepsilon_L(k) = 0. \qquad 49.$$

Solutions of the dispersion equations $\omega(\mathbf{k})$, with a generally complex frequency ω, represent plasma modes, which classically are, as already mentioned, the waves of electric and/or magnetic fields in the plasma, whereas quantum mechanically the modes are quasi-particle excitations of the plasma system. If the imaginary part of the mode's frequency $\Im\omega$ is negative, the mode is damped. Its amplitude decays exponentially in time as $e^{\Im\omega t}$. When $\Im\omega = 0$, we have a stable mode with a constant amplitude. Finally, if $\Im\omega > 0$, the mode's amplitude grows exponentially in time; there is an instability.

When the electric field of a mode is parallel to its wave vector $\mathbf{k}$, the mode is termed longitudinal. A mode is termed transverse when the electric field is transverse to the wave vector. The Maxwell equations show that the longitudinal modes, also known as electric, are associated with electric-charge oscillations. The transverse modes, also known as magnetic, are associated with electric-current oscillations.

The collective (boson) modes in the equilibrium ultrarelativistic plasma are shown in **Figure 2**. There are longitudinal modes, also termed plasmons and transverse modes. Both start at zero momentum at the plasma frequency, which is identical to the thermal photon (or gluon) mass, $\omega_p = m_\gamma$. The dispersion relations lie above the light cone ($\omega > |\mathbf{k}|$), showing that the plasma waves are undamped (no Landau damping) in the high-temperature limit. As explained in Section 3.3.1, the Landau damping, which arises formally from the imaginary part of the polarization tensor given by Equation 7 at $\omega^2 < \mathbf{k}^2$, occurs when the energy of the wave is transferred to plasma particles moving with velocity equal to the phase velocity ($\omega/|\mathbf{k}|$) of the wave.

If the phase velocity is larger than the speed of light, such a transfer is obviously not possible.

3.2.1. Two-stream system. As an example of the rich spectrum of collective modes, we consider the two-stream system within the hydrodynamic approach when the effect of pressure gradients is neglected. Details of the analysis can be found in Reference 21. The dielectric tensor provided by the polarization tensor from Equation 28 is

$$\varepsilon^{ij}(\omega,\mathbf{k}) = \left(1-\frac{\omega_p^2}{\omega^2}\right)\delta^{ij} - \frac{4\pi}{\omega^2}\sum_\alpha \frac{q_\alpha^2\bar{n}_\alpha^2}{\bar{\varepsilon}_\alpha+\bar{p}_\alpha}\left[\frac{\bar{v}_\alpha^i k^j + \bar{v}_\alpha^j k^i}{\omega-\mathbf{k}\cdot\bar{\mathbf{v}}_\alpha} - \frac{(\omega^2-\mathbf{k}^2)\bar{v}_\alpha^i\bar{v}_\alpha^j}{(\omega-\mathbf{k}\cdot\bar{\mathbf{v}}_\alpha)^2}\right], \quad 50.$$

where $\mathbf{v}_\alpha$ is the hydrodynamic velocity related to the hydrodynamic four-velocity and $\bar{u}_\alpha^\mu$. ω_p is the plasma frequency given as

$$\omega_p^2 \equiv 4\pi\sum_\alpha \frac{q_\alpha^2\bar{n}_\alpha^2}{\bar{\varepsilon}_\alpha+\bar{p}_\alpha}. \quad 51.$$

The index α, which labels the streams and plasma components, has four values, $\alpha = L-, L+, R-, R+$. The first character labels the stream (R for right and L for left), while the second one labels the plasma component ($+$ for positive and $-$ for negative charges). For simplicity we assume here that the streams are neutral and identical to each other and their velocities, which are chosen along the z-axis, and are opposite to each other. Then,

$$\begin{aligned}
&\bar{n} \equiv \bar{n}_{L-} = \bar{n}_{L+} = \bar{n}_{R-} = \bar{n}_{R+}, \quad \bar{\varepsilon} \equiv \bar{\varepsilon}_{L-} = \bar{\varepsilon}_{L+} = \bar{\varepsilon}_{R-} = \bar{\varepsilon}_{R+},\\
&\bar{p} \equiv \bar{p}_{L-} = \bar{p}_{L+} = \bar{p}_{R-} = \bar{p}_{R+}, \quad \bar{v} \equiv \bar{v}_{L-} = \bar{v}_{L+} = -\bar{v}_{R-} = -\bar{v}_{R+},\\
&e = q_{L-} = -q_{L+} = q_{R-} = -q_{R+}, \qquad 52.
\end{aligned}$$

and the plasma frequency is $\omega_p^2 = 16\pi e^2\bar{n}^2/(\bar{\varepsilon}+\bar{p})$.

The wave vector is first chosen to be parallel to the x-axis, $\mathbf{k} = (k, 0, 0)$. Owing to Equation 52, the off-diagonal elements of the matrix in Equation 48 vanish and the dispersion equation with the dielectric tensor given by Equation 50 is

$$\left(\omega^2-\omega_p^2\right)\left(\omega^2-\omega_p^2-k^2\right)\left(\omega^2-\omega_p^2-k^2-\lambda^2\frac{k^2-\omega^2}{\omega^2}\right) = 0, \quad 53.$$

where $\lambda^2 \equiv \omega_p^2\bar{v}^2$. As solutions of the equation, one finds a stable longitudinal mode with $\omega^2 = \omega_p^2$ and a stable transverse mode with $\omega^2 = \omega_p^2 + k^2$. There are also transverse modes with

$$\omega_\pm^2 = \frac{1}{2}\left[\omega_p^2-\lambda^2+k^2 \pm \sqrt{\left(\omega_p^2-\lambda^2+k^2\right)^2+4\lambda^2k^2}\right]. \quad 54.$$

As seen, $\omega_+^2 > 0$, but $\omega_-^2 < 0$. Thus, the mode ω_+ is stable and there are two modes with pure imaginary frequency corresponding to $\omega_-^2 < 0$. The first mode is overdamped, whereas the second one is the well-known unstable Weibel mode (43), leading to the filamentation instability. A physical mechanism of the instability is explained in Section 3.3.2.

The wave vector, as well as the stream velocities, is now chosen along the z-axis, i.e., $\mathbf{k} = (0, 0, k)$. Then, the matrix in Equation 48 is diagonal. With the dielectric tensor given by Equation 50, the dispersion equation reads

$$\left(\omega^2 - \omega_p^2 - k^2\right)^2 \left\{\omega^2 - \omega_p^2 - \omega_p^2 \left[\frac{k\bar{v}}{\omega - k\bar{v}} + \frac{(k^2 - \omega^2)\bar{v}^2}{2(\omega - k\bar{v})^2} - \frac{k\bar{v}}{\omega + k\bar{v}} + \frac{(k^2 - \omega^2)\bar{v}^2}{2(\omega + k\bar{v})^2}\right]\right\} = 0. \quad 55.$$

There are two transverse stable modes with $\omega^2 = \omega_p^2 + k^2$. The longitudinal modes are solutions of the above equation, which can be rewritten as

$$1 - \omega_0^2 \left[\frac{1}{(\omega - k\bar{v})^2} + \frac{1}{(\omega + k\bar{v})^2}\right] = 0, \quad 56.$$

where $\omega_0^2 \equiv \omega_p^2/2\bar{\gamma}^2$ with $\bar{\gamma} = (1 - \bar{v}^2)^{-1/2}$. With the dimensionless quantities $x \equiv \omega/\omega_0$ and $y \equiv k\bar{v}/\omega_0$, Equation 56 is

$$(x^2 - y^2)^2 - 2x^2 - 2y^2 = 0, \quad 57.$$

and is solved by

$$x_\pm^2 = y^2 + 1 \pm \sqrt{4y^2 + 1}. \quad 58.$$

As seen, x_+^2 is always positive and thus gives two real (stable) modes, x_-^2 is negative for $0 < y < \sqrt{2}$, and so there are two pure imaginary modes. The unstable one corresponds to the two-stream electrostatic instability. A physical mechanism of the instability is explained in Section 3.3.1.

3.3. Instabilities

The presence of unstable modes in a plasma system crucially influences its dynamics. Huge difficulties encountered by the half-century program to build a thermonuclear reactor are related to various instabilities experienced by a plasma, which make the system's behavior very turbulent, hard to predict, and hard to control.

There exists a large variety of instabilities; the history of plasma physics is said to be a history of discoveries of new instabilities. Plasma instabilities can be divided into two general groups: (*a*) hydrodynamic instabilities, caused by coordinate space inhomogeneities, and (*b*) kinetic instabilities due to the nonequilibrium momentum distribution of plasma particles.

The hydrodynamic instabilities are usually associated with phenomena occurring at the plasma boundaries. In the case of the QGP, this is the domain of highly nonperturbative QCD, where the non-Abelian nature of the theory is of crucial importance. Then, the behavior of the QGP is presumably very different from that of the EMP, and thus we will not speculate about possible analogies.

The kinetic instabilities are simply the collective modes with positive $\Im\omega$, introduced in Section 3.2 and found in Section 3.2.1 in the specific case of the two-stream system. Thus, we have longitudinal (electric) and transverse (magnetic) instabilities. In the nonrelativistic plasma, the electric instabilities are usually much more important than the magnetic ones, as the magnetic effects are suppressed by the factor v^2/c^2, where v is the particle's velocity. In the relativistic plasma, both types of instabilities

are of similar strength. As we discuss below, the electric instabilities occur when the momentum distribution of plasma particles has more than one maximum, as in the two-stream system. A sufficient condition for the magnetic instabilities appears to be an anisotropy of the momentum distribution.

3.3.1. Mechanism of electric instability. Let us consider a plane wave for the electric field, with the wave vector along the z-axis. For a charged particle, which moves with a velocity $v = p_z/E_p$ equal to the phase velocity of the wave $v_\phi = \omega/k$, the electric field does not oscillate, but is constant. The particle is then either accelerated or decelerated depending on the field's phase. For an electron with $v = v_\phi$, chances of being accelerated and decelerated are equal, as the time intervals spent by the particle in the acceleration zone and in the deceleration zone are the same.

Let us now consider electrons with velocities somewhat smaller than the phase velocity of the wave. Such particles spend more time in the acceleration zone than in the deceleration zone, and the net result is that the particles with $v < v_\phi$ are accelerated. Consequently, energy is transferred from the electric field to the particles. The particles with $v > v_\phi$ spend more time in the deceleration zone than in the acceleration zone, and thus they are effectively decelerated. Energy is transferred from the particles to the field. If the momentum distribution is such that there are more electrons in a system with $v < v_\phi$ than with $v > v_\phi$, the wave loses energy that is gained by the particles, as shown in the left graph of **Figure 3**. This is the mechanism of the famous collisionless Landau damping of the plasma oscillations. If there are more particles with $v > v_\phi$ than with $v < v_\phi$, the particles lose energy that is gained by the wave, as in the right graph of **Figure 3**. Consequently, the wave amplitude grows. This is the mechanism of electric instability. As explained above, it requires the existence of the momentum interval where $f_n(\mathbf{p})$ grows with $\mathbf{p}$. Such an interval appears when the momentum distribution has more than one maximum. This happens in the two-stream system discussed in Section 3.2.1 or in the system of a plasma and a beam, shown in **Figure 4**.

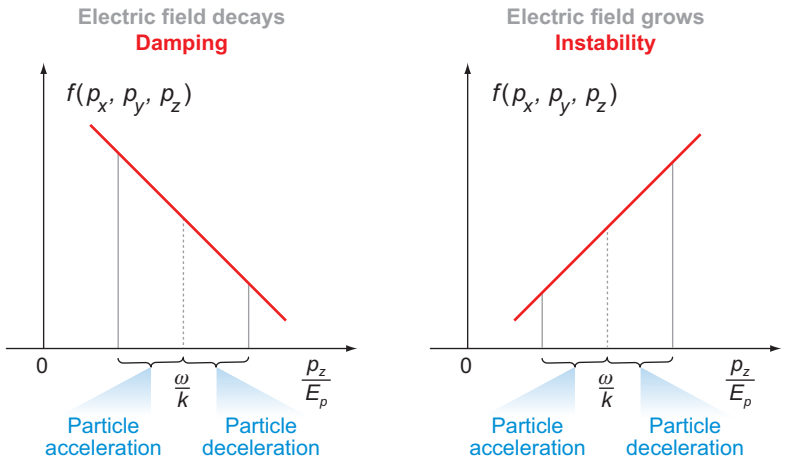

Figure 3
Mechanism of energy transfer between particles and fields.

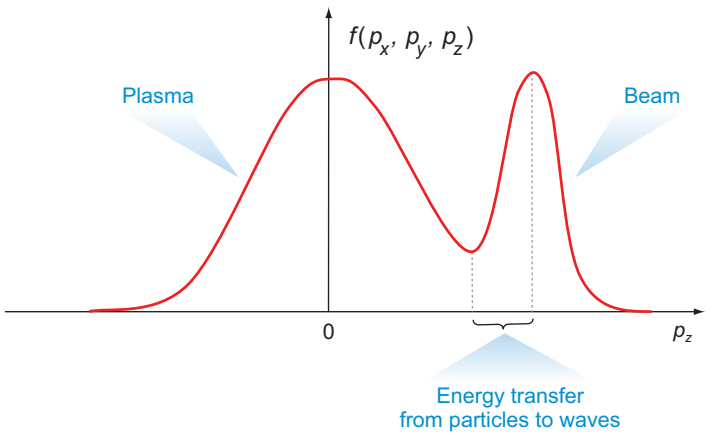

Figure 4
Momentum distribution of the plasma-beam system.

3.3.2. Mechanism of magnetic instability. Because the magnetic instabilities appear to be relevant for QGPs produced in relativistic heavy-ion collisions (see below), we discuss them in more detail. Let us first explain following Reference 44 how the unstable transverse modes are initiated. For this purpose we consider a plasma system that is homogeneous, but where the momentum distribution of particles is not of equilibrium form—it is not anisotropic. The system is on average locally neutral [$\langle j^\mu(x)\rangle = 0$] but current fluctuations are possible, and thus in general the correlator $\langle j^\mu(x_1)j^\nu(x_2)\rangle$ is nonzero. Because the plasma is assumed to be weakly coupled, the correlator can be estimated neglecting the interaction entirely. Then, when the effects of quantum statistics are also neglected, the correlator is

$$M^{\mu\nu}(t,\mathbf{x}) \stackrel{\text{def}}{=} \langle j^\mu(t_1,\mathbf{x}_1)j^\nu(t_2,\mathbf{x}_2)\rangle = \sum_n q_n^2 \int \frac{d^3p}{(2\pi)^3} \rightleftharpoons \frac{p^\mu p^\nu}{E_p^2} f_n(\mathbf{p})\delta^{(3)}(\mathbf{x}-\mathbf{v}t), \quad 59.$$

where $\mathbf{v} \equiv \mathbf{p}/E_p$ and $(t,\mathbf{x}) \equiv (t_2 - t_1, \mathbf{x}_2 - \mathbf{x}_1)$. Owing to the average space-time homogeneity, the correlator given by Equation 59 depends only on the difference $(t_2 - t_1,\ \mathbf{x}_2 - \mathbf{x}_1)$. The space-time points $(t_1,\ \mathbf{x}_1)$ and $(t_2,\ \mathbf{x}_2)$ are correlated in the system of noninteracting particles if a particle travels from $(t_1,\ \mathbf{x}_1)$ to $(t_2,\ \mathbf{x}_2)$. For this reason, the delta function $\delta^{(3)}(\mathbf{x}-\mathbf{v}t)$ is present in Equation 59. The sum and momentum integral represent summation over all particles in the system. The fluctuation spectrum is found as the Fourier transform of Equation 59; that is,

$$M^{\mu\nu}(\omega,\mathbf{k}) = \sum_n q_n^2 \int \frac{d^3p}{(2\pi)^3} \frac{p^\mu p^\nu}{E_p^2} f_n(\mathbf{p}) 2\pi\delta(\omega - \mathbf{k}\mathbf{v}). \quad 60.$$

To further study the fluctuation spectrum, the particle's momentum distribution must be specified. We present here only a qualitative discussion of Equations 59 and 60, assuming that the momentum distribution is strongly elongated in one direction, which is chosen to be along the z-axis. Then, the correlator M^{zz} is larger than M^{xx} or M^{yy}. It is also clear that M^{zz} is at its largest when the wave vector $\mathbf{k}$ is along the direction of the momentum deficit. In such a case the delta function $\delta(\omega - \mathbf{k}\mathbf{v})$ does not much constrain the integral in Equation 60. Because the momentum distribution

is elongated in the z-direction, the current fluctuations are at their largest when the wave vector $\mathbf{k}$ is in the x-y plane. Thus, we conclude that some fluctuations in the anisotropic system are large, much larger than in the isotropic one. An anisotropic system has a natural tendency to split into the current filaments parallel to the direction of the momentum surplus. These currents are seeds of the transverse unstable mode known as the filamentation, or Weibel, instability (43), which was found in the two-stream system discussed in Section 3.2.1.

Let us now explain in terms of elementary physics why the fluctuating currents, which flow in the direction of the momentum surplus, can grow in time. The form of the fluctuating current is chosen to be

$$\mathbf{j}(x) = j\,\hat{\mathbf{e}}_z\,\cos(k_x x), \qquad 61.$$

where $\hat{\mathbf{e}}_z$ is a unit vector in the z-direction. As seen in Equation 61, there are current filaments of the thickness $\pi/|k_x|$, with the current flowing in opposite directions in the neighboring filaments. The magnetic field generated by the current from Equation 61 is given as

$$\mathbf{B}(x) = 4\pi\,\frac{j}{k_x}\,\hat{\mathbf{e}}_y\,\sin(k_x x),$$

and the Lorentz force acting on the particles, which fly along the z-direction, is

$$\mathbf{F}(x) = q\,\mathbf{v}\times\mathbf{B}(x) = -4\pi q\,v_z\frac{j}{k_x}\hat{\mathbf{e}}_x\,\sin(k_x x),$$

where q is the particle's electric charge. One observes (see **Figure 5**) that the force distributes the particles in such a way that those that contribute positively to the current in a given filament are focused in the filament center, whereas those that contribute negatively are moved to the neighboring one. Thus, the initial current is growing and the magnetic field generated by this current is growing as well. The instability is driven by the energy transferred from the particles to fields. More specifically, the kinetic energy related to the motion along the direction of the momentum surplus is used to generate the magnetic field.

3.3.3. Role of instabilities. As mentioned above, there exists a large variety of plasma instabilities that strongly influence numerous plasma characteristics. Not much is known of the hydrodynamic instabilities of the QGP, and if they exist, they belong to the highly nonperturbative sector of QCD, which is still poorly understood. As explained in Section 3.3.1, the electric instabilities occur in a two-stream system, or more generally, in systems with a momentum distribution having more than one maximum. Although such a distribution is common in EMPs, it is rather irrelevant for QGPs produced in relativistic heavy-ion collisions, where the global as well as local momentum distributions are expected to monotonously decrease in every direction from the maximum. The electric instabilities are absent in such a system, but a magnetic unstable mode, which has been discussed in Section 3.3.2, is possible. The filamentaion instability was first argued to be relevant for the QGP produced in relativistic heavy-ion collisions in References 44–46. A characteristic time of

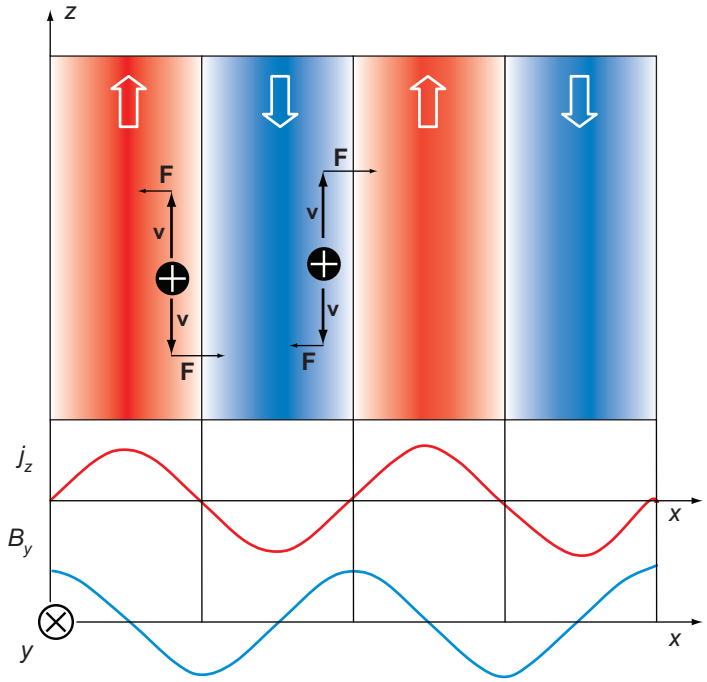

Figure 5

The mechanism of filamentation instability. See text for a description.

instability growth was estimated (45, 46) to be shorter or at least comparable to other timescales of the parton-system evolution. The mechanism of instability growth was also clarified (44). The early arguments were substantiated in the forthcoming analytic calculations (47–49) and numerical simulations (50–54).

A main consequence of instabilities is a fast equilibration of the weakly coupled plasma. The problem is of particular interest because the experimental data on heavy-ion collisions, where QGP production is expected, suggest that an equilibration time of the parton system is below 1 fm/c (55). A whole scenario of instabilities-driven equilibration is reviewed in Reference 56. Here we mention only the main points, starting with an observation that collisions of charged particles are not very efficient in redistributing particle momenta, as the Rutherford cross section is strongly peaked at a small momentum transfer. One needs either many frequent but soft collisions or a few rare but hard collisions to substantially change a particle's momentum. As a result, the inverse time of collisional equilibration of the QGP is of the order $g^4 \ln(1/g)T$ (16), where T is the characteristic momentum of quarks or gluons. It appears that the momentum distribution approaches isotropy owing to instabilities within the inverse time of order gT (57). If $1/g \gg 1$, the collisional equilibration is obviously much slower. As discussed in Section 4, the situation changes in strongly coupled plasmas.

When the instabilities grow, the system becomes more and more isotropic (46, 57) because the Lorentz force changes the particle's momenta, and the growing fields carry an extra momentum. To explain the mechanism, let us assume that initially there is a momentum surplus in the z-direction. The fluctuating current flows in the

z-direction, with the wave vector pointing in the x-direction. Because the magnetic field has a y-component, the Lorentz force—which acts on partons flying along the z-axis—pushes the partons in the x-direction where there is a momentum deficit. The numerical simulation (52) shows that growth of the instabilities is indeed accompanied by the system's fast isotropization.

The system isotropizes not only owing to the effect of the Lorentz force, but also owing to the momentum carried by the growing field. When the magnetic and electric fields are oriented along the y- and z-axes, respectively, the Poynting vector points in the x-direction along the wave vector. Thus, the momentum carried by the fields is oriented in the direction of the momentum deficit of particles.

Although the scenario of instabilities-driven equilibration looks very promising, the problem of thermalization of QGPs produced in heavy-ion collisions is far from being settled. Schenke et al. (58) showed that interparton collisions, which have been modeled using the BGK collision term (10), reduce the growth of instabilities and thus slow down the process of equilibration. The equilibration is also slowed down owing to expansion of the QGP into vacuum (59, 60), which is a characteristic feature of QGPs produced in relativistic heavy-ion collisions. Finally, the late stage of instability development, when non-Abelian effects are crucially important, appears to be very complex (61, 62), and it is far from being understood.

As already mentioned, instabilities influence various plasma characteristics. In particular, turbulent magnetic fields generated in the systems, which are unstable with respect to transverse modes, are responsible for a reduction of plasma viscosity (63). Then, an anomalously small viscosity, which is usually associated with strongly coupled systems, can occur in weakly coupled plasmas as well. Recently, it has been argued (64, 65) that the mechanism of viscosity reduction is operative in the unstable QGP.

3.4. Energy Loss

A charged particle that moves across the plasma changes its energy owing to several processes (2). When the particle's energy (E) is comparable to the plasma temperature (T), the particle can gain energy owing to interactions with field fluctuations. (In context of the QGP, the problem was studied in Reference 66) A fast particle with $E \gg T$ loses energy, and dominant contributions come from collisions with other plasma particles and from radiation. In the following we discuss the energy loss of a fast particle, as the problem is closely related to jet quenching, which was suggested long ago as a signature for QGP formation in relativistic heavy-ion collisions (67, 68).

Let us start with the collisional energy loss. The particle's collisions are split into two classes: hard, with high-momentum transfer, corresponding to the collisions with plasma particles, and soft, with low-momentum transfer dominated by the interactions with plasma collective modes. The momentum is called soft when it is of order of the Debye mass, m_D, or smaller, and it is hard when it is larger than m_D.

The soft contribution to the energy loss, which can be treated classically, is often known as plasma polarization. It leads to the energy loss per unit time given by the

formula

$$\left(\frac{dE}{dt}\right)_{\text{soft}} = \int d^3x\, \mathbf{j}(x)\mathbf{E}(x), \qquad 62.$$

where $\mathbf{E}$ is the electric field induced in the plasma by the particle's current $\mathbf{j}$, which is of the form $\mathbf{j}(x) = q\mathbf{v}\delta^{(3)}(\mathbf{x} - \mathbf{v}t)$. The field can be calculated by means of the Maxwell equations. After eliminating the magnetic field, one finds the equation

$$\left[\varepsilon^{ij}(k) - \frac{\mathbf{k}^2}{\omega^2}\left(\delta^{ij} - \frac{k^i k^j}{\mathbf{k}^2}\right)\right] E_j(k) = \frac{4\pi}{i\omega} j^i(k).$$

Because we consider equilibrium plasma, which is isotropic, one introduces the longitudinal (ε_L) and transverse (ε_L) components of ε^{ij}. Then, Equation 62 can be manipulated to

$$\left(\frac{dE}{dx}\right)_{\text{soft}} = -\frac{4\pi i e^2}{v}\int \frac{d^3k}{(2\pi)^3}\left\{\frac{\omega}{\mathbf{k}^2\varepsilon_L(k)} + \frac{\mathbf{v}^2 - \omega^2/\mathbf{k}^2}{\omega[\varepsilon_T(k) - \mathbf{k}^2/\omega^2]}\right\}, \qquad 63.$$

which gives the energy loss per unit length. This formula describes the effect of medium polarization. However, three comments are in order here:

1. Equation 63 includes the charge self-interaction signaled by the UV divergence of the integral from Equation 63. The self-interaction is removed by subtracting from Equation 63 the vacuum expression with $\varepsilon_L = \varepsilon_T = 1$.
2. Poles of the function under the integral from Equation 63 correspond to the plasma collective modes as given by the dispersion from Equation 49. Therefore, the explicit expressions of ε_L and ε_L are not actually needed to compute the integral in Equation 63. The knowledge of the spectrum of quasi-particles appears to be sufficient.
3. Equation 63 is derived in the classical approximation, which breaks down for a sufficiently large $\mathbf{k}$. Therefore, an upper cutoff is needed. The interaction with $\mathbf{k}$ above the cutoff, which, as already mentioned, is of order of the Debye mass, should be treated as hard collisions with plasma particles.

The energy loss per unit length due to hard collisions is

$$\left(\frac{dE}{dx}\right)_{\text{hard}} = \sum_i \int \frac{d^3k}{(2\pi)^3} n_i(k)\ [\text{flux factor}] \int d\Omega \frac{d\sigma^i}{d\Omega}\nu, \qquad 64.$$

where the sum runs over particle species distributed according to $n_i(k)$, $\nu \equiv E - E'$ is the energy transfer, and $d\sigma^i/d\Omega$ is the respective differential cross section. Combining Equations 63 and 64, one finds the complete collisional energy loss. The calculations of the energy loss of a fast parton in the QGP along the lines presented above were performed in References 69 and 70. Systematic calculations of the collisional energy loss using the hard thermal loop resummation technique were given in References 71 and 72, with a result that is infrared finite, gauge invariant, and complete to leading order. Recently, the calculations of the collisional energy loss have been extended to anisotropic QGPs (73).

It was realized that a sizeable contribution to the quark's energy loss comes from radiative processes (74). The problem, however, appeared to be very complex because the quark's successive interactions in the plasma cannot be treated as independent

from each other, and there is a destructive interference of radiated gluons known as the Landau-Pomeranchuk-Migdal effect (75). There are numerous papers devoted to the radiative energy loss, and the whole problem is reviewed in Reference 76. A general conclusion of these studies is that the energy lost by a fast light quark depends quadraticaly (not linearly) on the path traversed in the QGP, since the radiative energy loss dominates over the collisional loss. Recent experiments at RHIC show (77, 78), however, that heavy quarks, whose radiative energy loss is significantly suppressed, are strongly decelerated in the QGP medium. It may suggest that the collisional energy loss should actually be enhanced as predicted theoretically in Reference 79.

4. STRONGLY COUPLED PLASMAS

Our discussion of the collective phenomena presented in Section 3 was limited to weakly interacting plasmas, with the coupling constant much smaller than unity. However, the QGP produced in ultrarelativistic heavy-ion collisions is presumably strongly coupled quark-gluon plasma (sQGP), as the temperature is never much larger than Λ_{QCD}, and the regime of asymptotic freedom is not reached. The QGP is certainly a strongly interacting system close to the confinement phase transition. There are indeed hints in the extensive experimental material collected at RHIC (80–83) that the matter produced at the early stage of nucleus-nucleus collisions is in the form of sQGP for a few femtometers per speed of light. In particular, the characteristics of elliptic flow and particle spectra, which are well described by ideal hydrodynamics, seem to indicate a fast thermalization and small viscosity of the plasma. Both features are naturally explained assuming a strong coupling of the plasma (55, 84–87).

Although a fast thermalization (56) as well as a small viscosity (64, 65) can also be explained by instabilities, the idea of sQGP must be examined. However, the theoretical tools presented in Section 2 implicitly or explicitly assume a small coupling constant, and they are of limited applicability. A powerful approach, which can be used to study sQGP is the lattice formulation of QCD (for a review, see Reference 88). However, lattice QCD calculations, which are mostly numerical, encounter serious problems in incorporating quark degrees of freedom. It is also very difficult to analyze time-dependent plasma characteristics.

Strongly coupled conformal field theories such as supersymmetric QCD can be studied by means of the so-called AdS/CFT duality (89). Although some very interesting results on the conformal QGP were obtained in this way (see, e.g., Reference 90 and references therein), the relevance of these results for the QGP governed by QCD—not supersymmetric QCD—is unclear. Thus, the question arises: What we can learn about sQGP from strongly coupled EMPs?

We first note that most EMPs in nature and technological applications are weakly coupled. That is, the interaction energy between the plasma particles is much smaller than their thermal (kinetic) energy. This is because strongly coupled plasmas require a high particle density and/or low temperature, at which usually strong recombination occurs and the plasma state vanishes. Exceptions are the ion component in white dwarfs, metallic hydrogen, and other states of dense warm matter in the interior

of giant planets; short-living dense plasmas produced by intense laser or heavy-ion beams; or in explosive shock tubes, dusty (or complex) plasmas, and two-dimensional electron systems in liquid helium (91–93). Therefore, it is a real challenge to study strongly coupled EMPs both theoretically and experimentally.

In nonrelativistic EMP, the interaction energy is given by the (screened) Coulomb potential. The Coulomb coupling parameter defined by

$$\Gamma = \frac{q^2}{aT} \qquad 65.$$

distinguishes between weakly coupled, $\Gamma \ll 1$, and strongly coupled, $\Gamma \gtrsim 1$, plasmas. Here, q is the particle charge, a the interparticle distance, and T the kinetic temperature of the plasma component (electrons, ions, charged dust grains) under consideration. In the case of a degenerate plasma, for example, the electron component in a white dwarf, the kinetic energy T is replaced by the Fermi energy. Owing to the strong interaction, the plasma can behave either as a gas or a liquid, or even a solid (crystalline) system.

The case of a one-component plasma (OCP) with a pure Coulomb interaction (a single species of charged particles in a uniform, neutralizing background) has been studied in great detail as a reference model for strongly coupled plasmas using simple models as well as numerical simulations (91). For $\Gamma > 172$, the plasma was shown to form regular structures (Coulomb crystallization) (94). Below this critical value, the OCP is in the supercritical state. For values of Γ larger than $\sim$50, it behaves like an ordinary liquid, whereas for small values below unity, it behaves like a gas. Only if Γ is large enough does the usual liquid behavior (Arrhenius' law for the viscosity, Stokes-Einstein relation between self-diffusion and shear viscosity, etc.) appear owing to caging of the particles (a single particle is trapped for some period of time in the cage formed by its nearest neighbors). For values of Γ smaller than approximately 50, caging is not sufficiently strong and the system shows complicated, not yet understood transport properties. However, the short-range ordering typical for liquids shows up already for $\Gamma > 3$ (95). A gas-liquid transition requiring a long-range attraction and a short-range repulsion, for example, Lennard-Jones potential, does not exist in the OCP with particles of like-sign charges.

In realistic systems with a screened Coulomb interaction (Yukawa potential), the phase diagram can be shown in the Γ-κ plane, where $\kappa = a/\lambda_D$ is the distance parameter, with λ_D being the Debye screening length. Numerical simulations based on molecular dynamics lead to the phase diagram shown in **Figure 6** (96).

The first quantity of interest of sQGP is the coupling parameter. In analogy to nonrelativistic EMP, it is defined as (97)

$$\Gamma = \frac{2Cg^2}{4\pi aT} = 1.5 - 5, \qquad 66.$$

where C is the Casimir invariant ($C = 4/3$ for quarks and $C = 3$ for gluons), $a \simeq 0.5$ fm is the interparticle distance, and $T \simeq 200$ MeV is the QGP temperature corresponding to a strong-coupling constant $g \simeq 2$. The factor 2 in the numerator comes from taking into account the magnetic interaction in addition to the static electric (Coulomb) interaction, which are of the same magnitude in ultrarelativistic

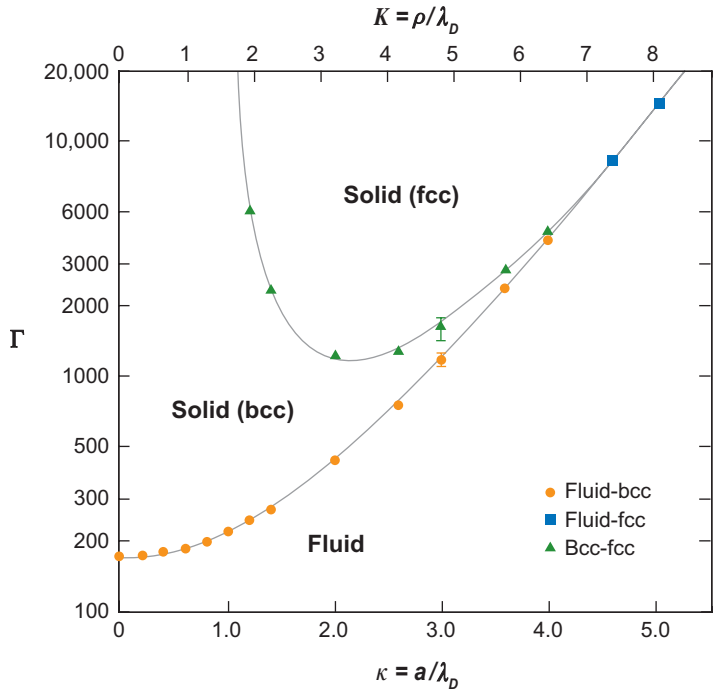

Figure 6

Phase diagram of a strongly coupled Yukawa system. Figure reprinted with permission from Reference 96. Copyright (1997) by the American Physical Society.

plasmas. The factor 4π in the denominator comes from using the Heaviside-Lorentz system in QCD, as discussed in the Introduction. The distance parameter κ of the QGP under the above conditions is rather small, typically between 1 and 3 (98).

Note that we have assumed here a classical interaction potential corresponding to one-gluon exchange. However, an effective potential that takes into account higher-order and nonperturbative effects may be much larger. This may be related to the fact that experimental data suggest a cross-section enhancement for the parton interaction by more than an order of magnitude (see below). Hence, the effective coupling parameter may be up to an order of magnitude larger than Equation 66.

As discussed above, comparison to the OCP model as well as experimental data suggests that QGPs close to the confinement phase transition could be in a liquid phase. The question arises whether there is a phase transition from a liquid to a gaseous QGP, as sketched in **Figure 7**. For such a transition, a Lennard-Jones-type interaction between the partons is required. However, the parton interaction in perturbative QCD is either purely repulsive or attractive in the various interaction channels, for example, in the quark-antiquark or diquark channels. Owing to nonlinear effects caused by the strong coupling, however, attractive interactions can arise even in the case of like-sign charges (see, e.g., Reference 99), leading to Lennard-Jones-type potentials. Hence, a gas-liquid transition in the QGP with a critical point, proposed in Reference 87, cannot be excluded and deserves further investigation.

An important quantity, which is very useful in theoretical and experimental studies of strongly coupled systems on the microscopic level, in particular in fluid physics

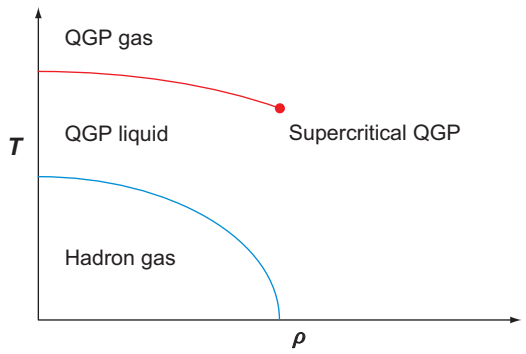

Figure 7

Sketch of a phase diagram of strongly interacting matter with a possible gas-liquid transition in the QGP phase. T denotes the temperature, while ρ is the baryon density.

(100), is correlation functions. In particular, the pair-correlation function and the static-structure function provide valuable information on the equation of state of the system (100). The extension of the approach to the QGP has been proposed in Reference 98.

The static density-density autocorrelation function is defined for a classical system as (91, 100)

$$G(\mathbf{r}) = \frac{1}{N}\int d^3r' \langle \rho(\mathbf{r}+\mathbf{r}', t)\rho(\mathbf{r}', t)\rangle,$$

where N is the total number of particles and

$$\rho(\mathbf{r},\ t) = \sum_{i=1}^{N} \delta^{(3)}(\mathbf{r} - \mathbf{r}_i(t))$$

is the local density of point particles, with $\mathbf{r}_i(t)$ denoting the position of i-th particle at time t. The density-density autocorrelation function is related to the pair-correlation function, which is defined as

$$g(\mathbf{r}) = \frac{1}{N}\left\langle \sum_{i,j,i\neq j}^{N} \delta^3(\mathbf{r}+\mathbf{r}_i - \mathbf{r}_j)\right\rangle$$

by the relation $G(\mathbf{r}) = g(\mathbf{r}) + \delta^{(3)}(\mathbf{r})$. The static-structure function, defined by

$$S(\mathbf{p}) = \frac{1}{N}\langle \rho(\mathbf{p})\rho(-\mathbf{p})\rangle,$$

with the Fourier-transformed particle density

$$\rho(\mathbf{p}) = \int d^3r \rho(\mathbf{r}) e^{-i\mathbf{p}\cdot\mathbf{r}},$$

is the Fourier transform of the density-density autocorrelation function

$$S(\mathbf{p}) = \int d^3r e^{-i\mathbf{p}\cdot\mathbf{r}} G(\mathbf{r})$$

The static-structure function $S(\mathbf{p})$ is constant for $\mathbf{p} \neq 0$ for uncorrelated particles (2). The typical behavior of the function in an interacting gas and in a liquid is sketched in **Figure 8**. The oscillatory behavior is caused by short-range correlations,

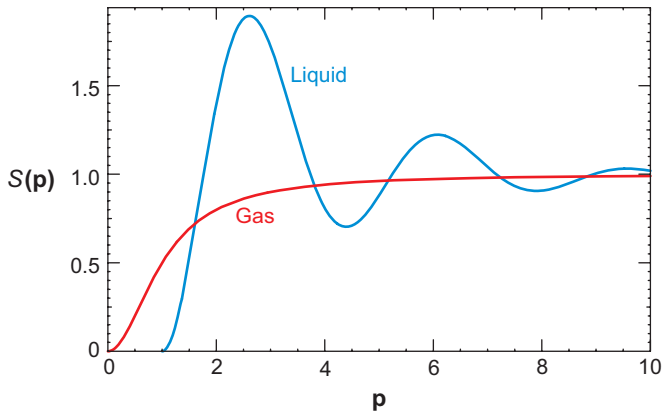

Figure 8

Sketch of the static-structure functions versus momentum in the gas and liquid phases in arbitrary units.

corresponding to a short-range ordering typical for liquids. In the case of an OCP, the oscillations appear for $\Gamma > 3$, indicating a liquid behavior (albeit with nonstandard transport properties) of the supercritical phase already for rather low values of Γ (95).

The static-quark structure function can be related to the longitudinal gluon-polarization tensor containing only the quark loop (**Figure 1**) via

$$S(\mathbf{p}) = -\frac{12}{\pi g^2 n}\int_0^\infty d\omega \Im\Pi_L(\omega, \mathbf{p}) \coth\frac{\omega}{2T},$$

where $n = N/V = \langle\rho(\mathbf{r})\rangle$ is the average particle density in a homogeneous system. As a reference for the strong-coupling regime, the static-quark structure function has been calculated in the weak-coupling limit by resumming the polarization tensor in the high-temperature limit (Equation 7), leading to (98)

$$S(\mathbf{p}) = \frac{2N_f T^3}{n}\frac{\mathbf{p}^2}{\mathbf{p}^2 + m_D^2}, \qquad 67.$$

where $m_D^2 = N_f g^2 T^2/6$ is the quark contribution to the Debye screening mass. The static-structure function given by Equation 67 starts at zero for $|\mathbf{p}| = 0$ and saturates at the uncorrelated structure function $S(\mathbf{p}) = 2N_f T^3/n$ for large $|\mathbf{p}|$. Such a structure function corresponds to an interacting Yukawa system in the gas phase (see **Figure 8**). Indeed, the pair-correlation function, following from the Fourier transform of $S(\mathbf{p}) - 1$, is

$$g(r) = -\frac{N_f T^3}{2\pi n}\frac{m_D^2}{r} e^{-m_D r},$$

and it reproduces the Yukawa potential.

To compute the structure function in strongly coupled plasmas, molecular dynamics is used (91). Although QGP is not a classical system, as the thermal de Broglie wave length is of the same order as the interparticle distance, molecular dynamics may be useful as a first estimate (87). Using molecular dynamics for a classical sQGP (101–103), the expected behavior described above has been qualitatively verified (101). In strongly coupled dense matter, where quantum effects are important,

quantum molecular dynamics based on a combination of classical molecular dynamics and density functional theory has been applied successfully (104). A generalization to the relativistic QGP has not been attempted so far. As an ultimate choice, lattice QCD could be used to calculate the structure or pair-correlation functions. This would provide a test for the state of sQGP as well as for the importance of quantum effects by comparing lattice results to classical molecular simulations.

As a last application, we consider the influence of strong coupling on the cross sections entering transport coefficients (shear viscosity), stopping power, and other dynamical quantities of the plasma. Besides higher-order and nonperturbative quantum effects, there is already a cross-section enhancement on the classical level. The reason is that the Coulomb radius, defined as $r_c = q^2/E$ for particle energy E, is of order of the Debye screening length—or r_c is even larger than λ_D in a strongly coupled plasma. Hence, the standard Coulomb scattering formula must be modified because the interaction with particles outside of the Debye sphere contributes significantly. Consequently, the inverse screening length cannot be used as an infrared cutoff. This modification leads, for example, to the experimentally observed enhancement of the so-called ion drag force in complex plasmas, which is caused by the ion-dust interaction (105).

In the QGP at $T \simeq 200$ MeV, the ratio r_c/λ_D equals 1–5. It may enhance a parton cross section by a factor of 2–9 (97) compared with perturbative results. An enhanced cross section reduces the mean free path λ and consequently reduces the viscosity η as $\eta \sim \lambda$. An enhancement of the elastic parton cross section by more than an order of magnitude compared with perturbative results also explains the elliptic flow and particle spectra observed at RHIC (106). An infrared cutoff smaller than the Debye mass provides a natural explanation for this enhancement. Also note that if the cross section is enhanced, the collisional energy loss grows. However, the radiative energy loss is expected to be suppressed in the sQGP by the Landau-Pomeranchuk-Migdal effect (75).

Finally, we mention two examples of strongly coupled systems that have not been considered in QGP physics but that may be of relevance. Strongly coupled plasmas such as two-dimensional Yukawa liquids (107) and dusty plasmas are non-Newtonian fluids. That is, the shear viscosity depends on the shear rate (flow velocity), as is observed in ketchup (shear thinning). The second example concerns nanofluidics. The expanding fireball in ultrarelativistic heavy-ion collisions has a transverse dimension of approximately 20 interparticle distances (approximately 10 fm). Fluids consisting of such a low number of layers exhibit properties different from large fluid systems. For example, the shear flow does not show a continuous velocity gradient but jumps owing to the adhesive forces between two layers. Such a behavior has been observed, for example, in complex plasmas.

LITERATURE CITED

1. Krall NA, Trivelpiece AW. *Principles of Plasma Physics*. New York: McGraw-Hill (1973)
2. Ichimaru S. *Basic Principles of Plasma Physics*. Reading: Benjamin (1973)

3. Hwa RC, ed. *Quark-Gluon Plasma*. Singapore: World Sci. (1990)
4. Hwa RC, ed. *Quark-Gluon Plasma 2*. Singapore: World Sci. (1995)
5. Hwa RC, Wang XN, eds. *Quark-Gluon Plasma 3*. Singapore: World Sci. (2004)
6. Mrówczyński St. *Acta Phys. Pol. B* 29:3711 (1998)
7. Blaizot JP, Iancu E. *Phys. Rep.* 359:355 (2002)
8. deGroot SR, Van Leeuwen WA, van Weert ChG. *Relativistic Kinetic Theory*. Amsterdam: North-Holland (1980)
9. Silin VP. *Sov. Phys. JETP* 11:1136 (1960)
10. Alexandrov AF, Bogdankovich LS, Rukhadze AA. *Principles of Plasma Electrodynamics*. Berlin: Springer (1984)
11. Carrington ME, Fugleberg T, Pickering D, Thoma MH. *Can. J. Phys.* 82:671 (2004)
12. Elze HT, Heinz UW. *Phys. Rep.* 183:81 (1989)
13. Mrówczyński St. *Phys. Rev. D* 39:1940 (1989)
14. Manuel C, Mrówczyński St. *Phys. Rev. D* 70:094019 (2004)
15. Schenke B, Strickland M, Greiner C, Thoma MH. *Phys. Rev. D* 73:125004 (2006)
16. Arnold P, Son DT, Yaffe LG. *Phys. Rev. D* 59:105020 (1999)
17. Manuel C, Mrówczyński St. *Phys. Rev. D* 68:094010 (2003)
18. Kolb PF, Heinz UW. In *Quark Gluon Plasma 3*, ed. RC Hwa, XN Wang, p. 634. Singapore: World Sci. (2004)
19. Huovinen P, Ruuskanen PV. *Annu. Rev. Nucl. Part. Sci.* 56:163 (2006)
20. Landau LD, Lifshitz EM. *Fluid Mechanics*. Oxford: Pergamon (1963)
21. Manuel C, Mrówczyński St. *Phys. Rev. D* 74:105003 (2006)
22. Kapusta JI. *Finite-Temperature Field Theory*. Cambridge: Cambridge Univ. Press (1989)
23. Le Bellac M. *Thermal Field Theory*. Cambridge: Cambridge Univ. Press (1996)
24. Schwinger JS. *J. Math. Phys.* 2:407 (1961)
25. Keldysh LV. *Zh. Eksp. Teor. Fiz.* 47:1515 (1964) [*Sov. Phys. JETP* 20:1018 (1965)]
26. Kadanoff LP, Baym G. *Quantum Statistical Mechanics*. New York: Benjamin (1962)
27. Bezzerides B, Dubois DF. *Ann. Phys.* 70:10 (1972)
28. Braaten E, Pisarski RD. *Nucl. Phys. B* 337:569 (1990)
29. Taylor JC, Wong SMH. *Nucl. Phys. B* 346:115 (1990)
30. Braaten E, Pisarski RD. *Phys. Rev. D* 45:1827 (1992)
31. Carrington ME, Hou D, Thoma MH. *Eur. Phys. J. C* 7:347 (1999)
32. Thoma MH. In *Quark-Gluon Plasma 2*, ed. RC Hwa, p. 51. Singapore: World Sci. (1995)
33. Pisarski RD. hep-ph/9710370 (1997)
34. Mrówczyński St, Thoma MH. *Phys. Rev. D* 62:036011 (2000)
35. Mrówczyński St, Rebhan A, Strickland M. *Phys. Rev. D* 70:025004 (2004)
36. Klimov VV. *Sov. Phys. JETP* 55:199 (1982)
37. Weldon HA. *Phys. Rev. D* 26:1394 (1982)
38. Blaizot JP, Iancu E. *Nucl. Phys. B* 417:608 (1994)
39. Kelly PF, Liu Q, Lucchesi C, Manuel C. *Phys. Rev. D* 50:4209 (1994)

40. Mustafa MG, Thoma MH, Chakraborty P. *Phys. Rev. C* 71:017901 (2005)
41. Ruppert J, Müller B. *Phys. Lett. B* 618:123 (2005)
42. Chakraborty P, Mustafa MG, Thoma MH. *Phys. Rev. D* 74:094002 (2006)
43. Weibel ES. *Phys. Rev. Lett.* 2:83 (1959)
44. Mrówczyński St. *Phys. Lett. B* 393:26 (1997)
45. Mrówczyński St. *Phys. Lett. B* 314:118 (1993)
46. Mrówczyński St. *Phys. Rev. C* 49:2191 (1994)
47. Randrup J, Mrówczyński St. *Phys. Rev. C* 68:034909 (2003)
48. Romatschke P, Strickland M. *Phys. Rev. D* 68:036004 (2003)
49. Arnold P, Lenaghan J, Moore GD. *JHEP* 0308:002 (2003)
50. Rebhan A, Romatschke P, Strickland M. *Phys. Rev. Lett.* 94:102303 (2005)
51. Arnold P, Lenaghan J. *Phys. Rev. D* 70:114007 (2004)
52. Dumitru A, Nara Y. *Phys. Lett. B* 621:89 (2005)
53. Arnold P, Moore GD, Yaffe LG. *Phys. Rev. D* 72:054003 (2005)
54. Rebhan A, Romatschke P, Strickland M. *JHEP* 0509:041 (2005)
55. Heinz U. *AIP Conf. Proc.* 739:163 (2005)
56. Mrówczyński St. *Acta Phys. Pol. B* 37:427 (2006)
57. Arnold P, Lenaghan J, Moore GD, Yaffe LG. *Phys. Rev. Lett.* 94:072302 (2005)
58. Schenke B, Strickland M, Greiner C, Thoma MH. *Phys. Rev. D* 73:125004 (2006)
59. Romatschke P, Venugopalan R. *Phys. Rev. Lett.* 96:062302 (2006)
60. Romatschke P, Rebhan A. *Phys. Rev. Lett.* 97:252301 (2006)
61. Arnold P, Moore GD. *Phys. Rev. D* 73:025013 (2006)
62. Dumitru A, Nara Y, Strickland M. hep-ph/0604149 (2006)
63. Abe T, Niu K. *J. Phys. Soc. Jpn.* 49:717 (1980)
64. Asakawa M, Bass SA, Müller B. *Phys. Rev. Lett.* 96:252301 (2006)
65. Asakawa M, Bass SA, Müller B. hep-ph/0608270 (2006)
66. Chakraborty P, Mustafa MG, Thoma MH. hep-ph/0611355 (2006)
67. Bjorken JD. *Fermilab preprint* 82/59-THY (1982)
68. Gyulassy M, Plümer M. *Phys. Lett. B* 243:432 (1990)
69. Thoma MH, Gyulassy M. *Nucl. Phys. B* 351:491 (1991)
70. Mrówczyński St. *Phys. Lett B* 269:383 (1991)
71. Braaten E, Thoma MH. *Phys. Rev. D* 44:R2625 (1991)
72. Braaten E, Thoma MH. *Phys. Rev. D* 44:1298 (1991)
73. Romatschke P, Strickland M. *Phys. Rev. D* 71:125008 (2005)
74. Gyulassy M, Wang XN. *Nucl. Phys. B* 420:583 (1994)
75. Landau LD, Pomeranchuk IY. *Dokl. Akad. Nauk. SSR* 92:535 (1953); Landau LD, Pomeranchuk IY. *Dokl. Akad. Nauk. SSR* 92:735 (1953); Migdal AB. *Phys. Rev.* 103:1811 (1956)
76. Baier R, Schiff D, Zakharov BG. *Annu. Rev. Nucl. Part. Sci.* 50:37 (2000)
77. Adler SS, et al. (PHENIX Collab.) *Phys. Rev. Lett.* 96:032301 (2006)
78. Abelev BI, et al. (STAR Collab.) nucl-ex/0607012 (2006)
79. Mustafa MG, Thoma MH. *Acta Phys. Hung. A* 22:93 (2005)
80. Arsene I, et al. (BRAHMS Collab.) *Nucl. Phys. A* 757:1 (2005)
81. Back BB, et al. (PHOBOS Collab.) *Nucl. Phys. A* 757:28 (2005)

82. Adams J, et al. (STAR Collab.) *Nucl. Phys. A* 757:102 (2005)
83. Adcox K, et al. (PHENIX Collab.) *Nucl. Phys. A* 757:184 (2005)
84. Gyulassy M, McLerran L. *Nucl. Phys. A* 750:30 (2005)
85. Shuryak EV. *Nucl. Phys. A* 774:387 (2006)
86. Cassing W, Peshier A. *Phys. Rev. Lett.* 94:172301 (2005)
87. Thoma MH. *Nucl. Phys. A* 774:307 (2006)
88. Karsch F. *Lect. Notes Phys.* 583:209 (2002)
89. Maldacena JM. *Adv. Theor. Math. Phys.* 2:231 (1998) [*Int. J. Theor. Phys.* 38:1113 (1999)]
90. Kovtun P, Son DT, Starinets AO. *Phys. Rev. Lett.* 94:111601 (2005); Janik RA, Peschanski R. *Phys. Rev. D* 74:046007 (2006)
91. Ichimaru S. *Rev. Mod. Phys.* 54:1017 (1982)
92. Fortov VE, et al. *Phys. Rep.* 421:1 (2005)
93. Tahir NA, et al. *J. Phys. A* 39:4755 (2006); Hoffmann DHH, et al. *J. Phys. IV* 133:49 (2006)
94. Slattery WL, Doolen GD, Witt HE. *Phys. Rev. A* 21:2087 (1980)
95. Daligault J. *Phys. Rev. Lett.* 96:065003 (2006)
96. Hamaguchi S, Farouki RT, Dubin DHE. *Phys. Rev. E* 56:4671 (1997)
97. Thoma MH. *J. Phys. G* 31:L7 (2005). Erratum. *J. Phys. G* 31:539 (2005)
98. Thoma MH. *Phys. Rev. D* 72:094030 (2005)
99. Tsytovich V. *Contrib. Plasma Phys.* 45:533 (2005)
100. Hansen JP, McDonald IR. *Theory of Simple Liquids*. London: Acad. Press (1986)
101. Gelman BA, Shuryak EV, Zahed I. *Phys. Rev. C* 74:044908 (2006)
102. Gelman BA, Shuryak EV, Zahed I. *Phys. Rev. C* 74:044909 (2006)
103. Hartmann P, Donko Z, Levai P, Kalman GJ. *Nucl. Phys. A* 774:881 (2006)
104. Car R, Parrinello M. *Phys. Rev. Lett.* 55:2471 (1985)
105. Yaroshenko V, et al. *Phys. Plasmas* 12:093503 (2005)
106. Molnar D, Gyulassy M. *Nucl. Phys. A* 697:495 (2002)
107. Donko Z, Goree J, Hartmann P, Kutasi K. *Phys. Rev. Lett.* 96:145003 (2006)